APPLICATION OF FLUORESCENCE TO UNDERSTAND THE INTERACTION OF PEPTIDES WITH BINARY LIPID MEMBRANES

Rodrigo F. M. de Almeida, Luís M. S. Loura, and Manuel Prieto*

12.1. INTRODUCTION

The fluid mosaic model of biological membranes (Singer and Nicolson, 1972) emphasizes membrane fluidity and free lateral diffusion of membrane components. This led to the generalized idea of biomembranes as solutions of proteins embedded in bilayers of randomly distributed phospholipids. However, over the past few decades, evidence has accumulated suggesting that the lipid distribution on the bilayer is nonrandom, both in model systems and in biological membranes (Edidin, 1998). In fact, it can exhibit ordered structures with length scales ranging from micrometers (visualized by microscopy; Korlach *et al.*, 1999) to nanometers (mostly indirect evidence, see Mouritsen and Jørgensen, 1997, for a review).

It has been long realized that model systems of membranes prepared with lipid mixtures with different main transition temperatures (T_m) can exhibit lateral phase coexistence of gel/fluid phases. Depending on the ideality of the mixture, gel-gel (*e.g.*, 1,2-dilauroyl-*sn*-glycero-3-phosphocholine (DLPC)/1,2-distearoyl-*sn*-glycero-3-phosphocholine (DSPC); Mabrey and Sturtevant, 1976) and even gel-gel and fluid-fluid (*e.g.*, 1,2-dielaydoyl-*sn*-glycero-3-phosphocholine (DEPC)/1,2-dipalmitoyl-*sn*-glycero-3-phosphoethanolamine (DPPE); Wu and McConnell, 1975) phase separation can occur. The fact that phase separation occurs for mixtures of lipids coexisting in cell membranes under conditions close to physiological (*e.g.*, Marsh, 1990) made the detection and characterization of this kind of lateral heterogeneity of considerable interest in the biophysical and biochemical communities (*e.g.*, Edidin, 2003). The composition-temperature phase diagrams, at constant pressure (and ionic strength, *etc.*), are a convenient way to represent this type of behavior for each pair of phospholipids. Considering lamellar and quasi-lamellar phases, namely the gel and fluid, the variety of phase diagrams (isomorphous, eutectic, peritectic, monotectic and eutectic) is similar to

* Rodrigo F. M. de Almeida, Luís M. S. Loura, and Manuel Prieto, Centro de Química-Física Molecular, Instituto Superior Técnico, 1049-001 Lisboa, Portugal. Luís M. S. Loura, Departamento de Química and Centro de Química, Universidade de Évora, 7000-671 Évora, Portugal.

other areas of Chemistry, as metallurgy (a good collection of phase diagrams for binary lipid mixtures is given by Marsh (1990)). Even in the absence of macroscopic phase separation in the fluid phase, a considerable degree of lateral heterogeneity can persist above the liquidus line. This was predicted in Monte-Carlo simulations (Mouritsen and Jørgensen, 1994) and experimentally confirmed by us by means of resonance energy transfer (FRET) (de Almeida *et al.*, 2002) for the highly non-ideal mixture of DLPC/DSPC.

In the case of binary lipid mixtures, the difference in T_m between the two components can arise from differences in the acyl chain length (*e.g.*, the already mentioned DLPC/DSPC) and/or degree of unsaturation (*e.g.*, DEPC/DSPC; Wu and McConnel, 1975) and different head groups. For this last case, let us consider the phase diagram for the mixture 1,2-dimyristoyl-*sn*-glycero-3-phosphocholine (DMPC)/ 1,2-dimyristoyl-*sn*-glycero-3-phosphate (DMPA) determined from differential scanning calorimetry (DSC) experiments by Graham *et al.* (1985). At low phosphatidic acid (PA) contents, the thermograms have a complex shape, as the pre-transition of the pure phosphatidylcholine (PC) species is not abolished. The phase diagram for the mixture is shown on Figure 12.1. The diagram is peritectic, with gel-gel and gel-fluid coexistence regions.

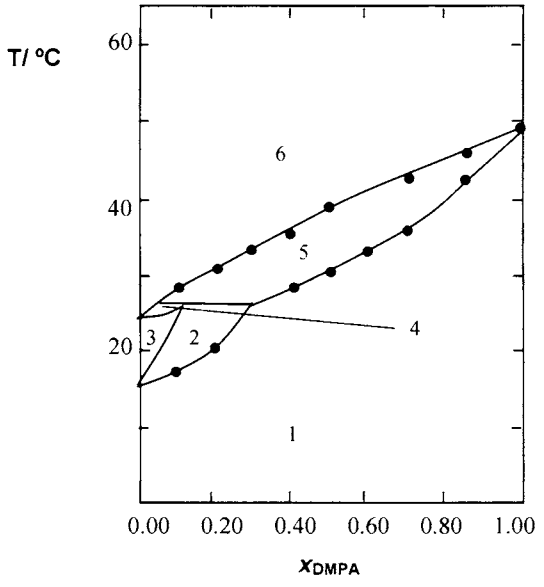

Figure 12.1. Phase diagram for the lipid mixture DMPC/DMPA. The different regions of the phase diagram are: 1) gel phase; 2) coexistence of gel rippled/gel phases; 3) gel rippled phase; 4) coexistence of gel rippled/fluid phases; 5) coexistence of fluid/gel phases; 6) fluid phase. Adapted from *Graham et al.* (1985).

The study of the interaction of model peptides with a zwitterionic lipid bilayer was fundamental to establish the hydrophilic/hydrophobic energetics of membrane proteins insertion (Wimley and White, 1996). Nonetheless, the importance of the complex

composition of natural membranes has long been realized, and the presence of a single additional component, *e.g.*, the use of a binary zwitterionic/anionic phospholipid mixture, is sufficient to allow for a multiplicity of interactions. Phase separation can be induced in a binary lipid mixture with composition and temperature where otherwise only one phase would be present, namely through addition of a positively charged molecule to a mixture of a zwitterionic and an anionic phospholipids at a certain pH. In the case of the mixture 1,2-dipalmitoyl-*sn*-glycero-3-fosfo-*rac*-glycerol (DPPG) with DMPC or DSPC phase separation can be induced by addition of the cationic peptide mellitin (Lafleur *et al.*, 1989). In sum, the following possibilities have to be considered: (*i*) phase behavior of the binary lipid mixture in the absence of peptide (knowledge of the temperature/composition phase diagram); (*ii*) influence of the peptide on the phase behavior (shifts in the phase diagram, creation of new regions/types of phase separation); and (*iii*) influence of the peptide on the phase separation topology. In fact, the formation of lipid domains is thought to be a key process in several biological functions (Welti and Glaser, 1994; Simons and Ikonen, 1997) and the clarification of the relationship between lipid domains and the binding and functional properties of membrane-associated proteins is an emerging area in membrane research (Johnson and Cornell, 1999; Hurley and Meyer, 2001).

Another group of lipid mixtures that have been intensely used are phospholipid (mainly PC)/cholesterol (chol) binary systems. These mixtures' properties and interaction with peptides and proteins is of importance due to the high abundance of chol in mammalian plasma membranes. From the studies in model systems important conclusions have been inferred about the role of sterols in biomembranes.

The well-known effects of chol on the bilayer properties (see, *e.g.*, Bloom e Mouritsen, 1995; Needham e Nunn, 1990) have been rationalized considering that in the presence of high amounts of chol in a PC bilayer, the membrane is in a liquid ordered (lo) phase (using the nomenclature introduced by Ipsen *et al.*, 1987), with properties midway between the gel and the fluid. This designation highlights the facts that the translational diffusion is closer to the fluid phase (the diffusion coefficient in the lo phase is only 2 to 3 times lower than for the pure fluid phase of the PC), but the acyl chains are in a much more ordered configuration. In this nomenclature, the gel and fluid phases are designated by solid ordered (so) and liquid disordered (ld), respectively. The phase diagram is monotectic and for intermediate chol concentrations phase coexistence occurs: so and lo, below the monotectic temperature (which is close to T_m) and ld with lo, above the monotectic temperature. The latter corresponds to fluid-fluid phase separation, which is thought to be of biological relevance, namely, to the raft phenomenon (*e.g.*, Brown e London (2000)). It should be mentioned that, for PC/chol systems, the most studied being DPPC/chol, there are several phase diagrams reported, that differ considerably among them (*e.g.*, Vist and Davis, 1990; Lentz *et al.*, 1980; McMullen and McElhaney, 1995). The discrepancies are probably related to the similarity between the two phases, which makes differentiation between them difficult (London and Brown, 2000). Nevertheless, some of those discrepancies have been rationalized (de Almeida *et al.*, 2003) and ld/lo phase separation is a suitable model for the examples presented in the present review.

Although not the most intensely studied, the mixture 1-palmitoyl-2-oleoyl-*sn*-glycero-3-phosphocholne (POPC)/chol is particularly relevant. In fact, POPC is a 1-saturated, 2-unsaturated PC, a common motif found in naturally occurring phospholipids, being the major lipid component in PC isolated from several natural sources (Marsh, 1990). It has a low T_m (Marsh, 1990), but it has the ability to form a lo phase in the

presence of chol both below (Thewalt and Bloom, 1992) and above (Mateo *et al.*, 1995) T_m, *i.e.*, so/lo and ld/lo phase coexistence, respectively. It is used in several studies in ternary (or higher) model systems (*e.g.*, Silvius, 1992; Milhiet *et al.*, 2001; Dietrich *et al.*, 2001; de Almeida *et al.*, 2003). The partial phase diagram POPC/chol is shown in Figure 12.2, where a broad ld/lo coexistence region can be observed. The phase diagram is similar to one previously published (Mateo *et al.*, 1995), except that for the lower temperatures the phase coexistence both begins and ends at slightly higher chol mole fractions (x_{chol}). This diagram was determined from fluorescence measurements, namely the lifetime and anisotropy of the fluorescent membrane probes 1,6-diphenyl-1,3,5-hexatriene (DPH) and *trans*-parinaric acid (*t*-PnA).

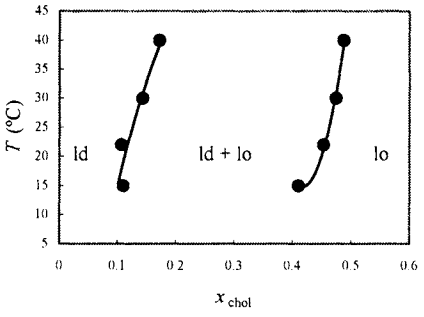

Figure 12.2. POPC/chol phase diagram. The experimental points were determined from fluorescence anisotropy and lifetimes of the lipophilic probes DPH and *t*-PnA. Reprinted from de Almeida *et al.* (2003) with permission. Copyright 2003 Biophysical Society.

After a recent review that surveys literature studies on the interaction of peptides with binary phospholipids membranes (Loura *et al.*, 2003), in the present article, we also address in a more general way lipid-protein interactions with not only phospholipid/phospholipid mixtures, but also with phospholipid/sterol mixtures, and studies in single lipid vesicles can be also addressed when considered particularly relevant. Instead of a comprehensive literature review, we illustrate the several fluorescence-based methodologies, highlighting the relevant information that can be extracted from their application, with studies carried out in our laboratory.

12.2. QUANTIFYING THE EXTENT OF INTERACTION OF THE PEPTIDE WITH THE MEMBRANE

The determination of the partition coefficient, K_p, is usually the first step in the study of the interaction of a peptide with model membranes, and should precede structural and dynamic studies. It allows quantifying the fraction of membrane bound peptide for a given lipid concentration, and it gives a measure of the "strength" of the peptide-membrane interaction, permitting, *e.g.*, quantitative comparison between different lipid species and/or phases. It is defined by (for an alternative definition and interconversion see Santos *et al.*, 2003; Loura *et al.*, 2003)

$$K_p = \frac{n_{S,L}/V_L}{n_{S,W}/V_W} \tag{1}$$

where V_i are the volumes of the phases, and $n_{S,i}$ are the moles of solute present in each phase (i = W, aqueous phase; i = L, lipid phase). An equivalent equation is obtained by expressing the membrane-bound peptide mole fraction, x_L, as a function of the lipid concentration, [L]:

$$x_L = \frac{K_p \bar{V}_L [L]}{K_p \bar{V}_L [L] + 1} \tag{2}$$

where $\bar{V}_L$ is the molar volume of the lipid phase.

For most cases, the partition coefficient of a molecule between a lipid and an aqueous phase can be obtained by fluorescence spectroscopy as long as there is a difference in a fluorescence parameter of the partitioning molecule (*e.g.*, quantum yield, fluorescence anisotropy or fluorescence lifetime) when in aqueous solution and after incorporation in the membrane (or, less commonly for peptides, if the incorporation of the molecule in the membrane leads to a change on a fluorescence property of a membrane probe). Fluorescence emission intensity, I, and steady-state anisotropy, $<r>$ (Section 12.5), can both be used to calculate the partition coefficient of a fluorescent molecule between lipid and aqueous phases:

$$I = \frac{I_W + I_L K_p \bar{V}_L [L]}{1 + K_p \bar{V}_L [L]} \tag{3}$$

$$< r >= \frac{< r >_W + < r >_L K_p \bar{V}_L [L] \varepsilon_L \Phi_L / (\varepsilon_L \Phi_L)}{1 + K_p \bar{V}_L [L] \varepsilon_L \Phi_L / (\varepsilon_L \Phi_L)} \tag{4}$$

where $\bar{V}_L$ is the lipid molar volume, ε_i is the molar absorption coefficient at the excitation wavelength and Φ_i is the fluorescence quantum yield of the peptide in phase i. In Eq. (3), the lifetime-weighted quantum yield, $<\tau>$, readily obtained from the fluorescence decay lifetimes τ_i and respective normalized amplitudes a_i from (*e.g.*, Engelborghs, 2001)

$$< \tau >= \sum_i a_i \tau_i \tag{5}$$

can be used instead of I through the relationship:

$$\langle \tau \rangle = \frac{\langle \tau \rangle_W + \langle \tau \rangle_L K_p \bar{V}_L [L]}{1 + K_p \bar{V}_L [L]} \tag{6}$$

(note that both $<\tau>$ and I are proportional to the fluorescence quantum yield). In fact, the use of data coming from time-resolved experiments is less prone to artifacts such as light scattering or inner filter effects, and is preferred to the use of steady-state intensities. Anisotropy measurements are also strongly affected by light scattering, which can be critical for the highest lipid concentrations such as shown in, *e.g.*, Figure 12.8 of Castanho and Prieto (1992). This eventually is the greatest restriction to the otherwise very sensitive fluorescence technique, because for a correct recovery of the lipid-phase parameter I_L, r_L or $<\tau>_L$ (and also K_p, due the strong correlation of the two parameters), a quasi-plateau region on the plots should be obtained. Bimolecular photophysical interactions involving peptide molecules, such as self-quenching and energy homotransfer are eventual complicating factors, mainly for situation of overcharged membranes.

The spectroscopic determinations are usually carried out by titration, *i.e.*, addition of successive amounts of lipid to the solution keeping the solute concentration constant (except for the dilution effect). However, tryptophan (Trp) and tyrosine (Tyr) are prone to photobleaching, and, in such case, preparation of separate samples with constant solute concentrations and different lipid amounts should be considered. This procedure was used to determine the partition coefficient of the peptide comprising the residues 579-601 of gp41 ectodomain from the human immunodeficiency virus type-1 (HIV-1) between water and lipid vesicles of POPC/1,2-dimyristoyl-*sn*-glycero-3-phosphoglycerol (DMPG) 8:2 (Santos *et al.*, 1998). As shown in Figure 12.3, the fluorescence intensity of the Trp residue increases with lipid concentration. In the top panel, steady-state intensities were used, and in the bottom panel, the lifetime-weighted quantum yield approach was employed. The trend of the data is analogous, and in fact the recovered partition coefficients are of the same order of magnitude. Clearly, the time-resolved data are of better quality than the steady-state data, as mentioned above, when high lipid concentrations have to be reached. The relative error associated to the recovered K_p value is reduced from 57% (steady-state data) to 32% (time-resolved data).

In case that K_p is not too high, the molar fraction of solute in water, $x_W = 1 - x_L$, can be significant. If the solute fluoresces in water (*e.g.*, Trp), the experimental spectrum, $I(\lambda)_{L+W}$, is the sum of the fractions in water, $I(\lambda)_W$, and in the membrane, $I(\lambda)_L$. The latter one can be obtained from Eq. (7):

$$I(\lambda)_L = C \cdot \left(I(\lambda)_{L+W} - x_W \frac{1}{1 + <\tau>_L / <\tau>_W} I(\lambda)_W \right) \tag{7}$$

Similarly to the fluorescence spectra, the total anisotropy decay is often difficult to analyze. In the most common case of complex decay (two or more components) for peptides, the number of needed fitting parameters would be too large. However, even in the case that the dynamic information contained in the initial part of the decay cannot be recovered, the limiting anisotropy of the bound species, $r_{\infty,L}$, which allows an easy determination of the order parameter of the system (Section 12.5), is readily obtained:

$$r_\infty^L = \left(1 + \frac{x_W \langle\tau\rangle_W}{x_L \langle\tau\rangle_L} \right) \cdot r_\infty \tag{8}$$

where r_∞ is the experimentally determined value in the presence of lipid at time → ∞.

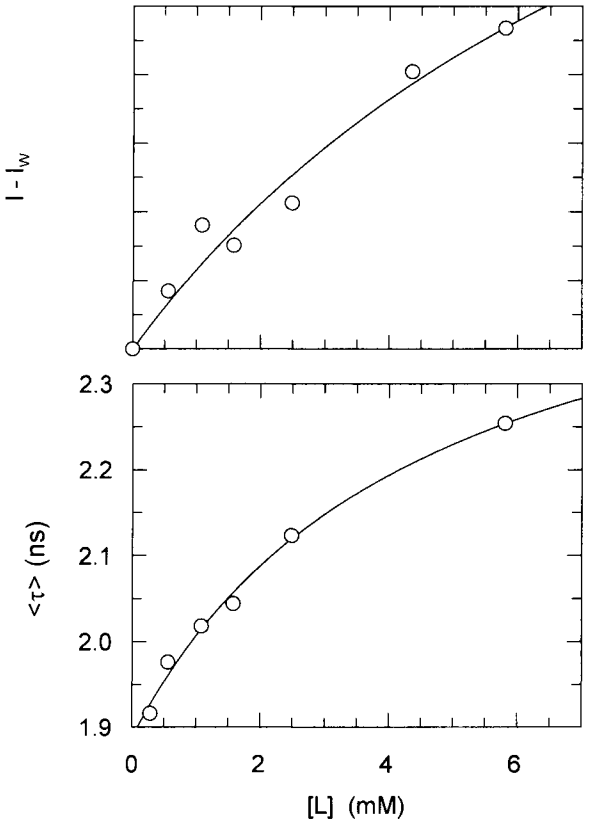

Figure 12.3. Determination of the partition constant (K_p) of the peptide comprising the residues 579-601 of gp41 ectodomain of HIV-1 between the aqueous phase and phospholipid vesicles. Peptide concentration was constant during each set of experiments. Increase in fluorescence intensity (I - I_W) obtained for different concentrations of POPC/DMPG 80:20 small unilamellar vesicles (SUV) (top), and fitting lines calculated using Eq. (3). Lifetime weighted quantum yield <τ> obtained for different concentrations of POPC/DMPG 80:20 SUV (bottom), and fitting lines calculated using Eq. (6). Reprinted with permission from Santos *et al.* (1998). Copyright 1998 American Chemical Society.

As an illustration of the use of these latter equations, we shall consider the interaction of the positively charged peptide α-MSH, a hormone known for its role in regulating skin pigmentation in vertebrates (Eberle, 1988) with both DMPC (zwitterionic)/DMPG (anionic) and DMPC/DMPA (anionic) (both 3:1 mixtures), which was studied using complementary techniques (DSC, infrared and ultraviolet absorption spectroscopy, and steady-state and time resolved fluorescence; Contreras *et al.*, 2001). Figure 12.4 shows the emission spectra at 20°C recovered using Eq. (7), whereas Table 12.1 shows the recovered blue-shifts relative to buffer, as well as the recovered limiting anisotropies $r_{\infty,L}$, both at 20°C and 37°C. Interestingly, a larger blue-shift is observed for DMPC/DMPG in the fluid phase relative to the gel (pointing to a deeper location of the

Trp residue in the fluid bilayer), whereas the opposite is observed for DMPC/DMPA. On the other hand, high values (for a non-transmembrane helix) of $r_{\infty,L}$ are obtained, meaning that the peptide is strongly adsorbed at the interface and highly immobilized.

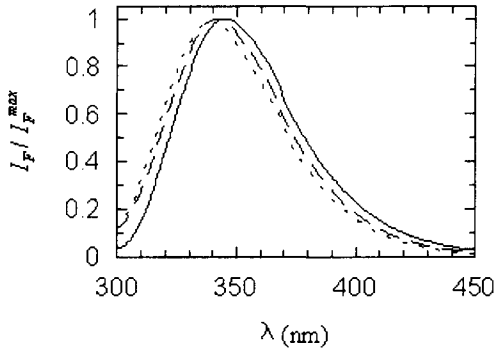

Figure 12.4. Corrected fluorescence emission spectra (λ_{exc} = 290 nm) of α-MSH at 20°C in aqueous solution (——), incorporated in gel phase large unilamellar vesicles (LUV) of DMPC/DMPG (3:1) (— —), and DMPC/DMPA (3:1) (- - - -). The spectra were corrected using Eq. (7) as described in the text. Reprinted from Contreras *et al.* (2001) with permission. Copyright 2001 Biophysical Society.

Table 12.1. Lipid/water partition coefficients (K_p), and ^{9}Trp photophysical parameters of α-MSH in different systems: $<\tau>$ - lifetime-weighted quantum yield; $\Delta\lambda$ - membrane /water spectral-shift; r_∞ - limiting anisotropy.

System	T (°C)	$K_p^{(lipid/water)}/10^2$	$<\tau>_{W \text{ or } L}$ (ns)	$\Delta\lambda$ (nm)	$r_\infty^{W \text{ or } L}$
Buffer	20	-----	2.21 ± 0.02	-----	0
(W)	37	-----	1.51 ± 0.03	-----	0
DMPC/DMPG (3:1)	20	2.8 ± 0.2	3.22 ± 0.05	3.0	0.125 ± 0.006
(L)	37	4.0 ± 1.4	2.44 ± 0.16	5.0	0.090 ± 0.015
DMPC/DMPA (3:1)	20	6.0 ± 1.8	2.60 ± 0.05	6.0	0.127 ± 0.021
(L)	37	3.5 ± 1.0	2.25 ± 0.11	5.0	0.114 ± 0.017

Reprinted from Contreras *et al.* (2001) with permission. Copyright 2001 Biophysical Society.

In addition to water/lipid partition, one can define the partition coefficient between the two lipid phases that eventually coexist in binary lipid mixtures, identically to Eq. (1), and the same methodologies as described above can be used for its determination (in that case, values of K_p close to unity denote essentially random distribution of peptide between the two lipid phases, and K_p significantly different from unity denotes strong preference for one particular phase). However, this type of study is most uncommon for peptides, possibly because most of these have the additional complexity of significant

partition to the aqueous phase. Commonly, a single aqueous phase/lipid bilayer K_p value is determined, which must be seen as a complex average between the not necessarily identical K_p values for partition between the aqueous medium and each lipid phase. Even on the frame of this simplification, useful information can be obtained. For example, returning to the aforementioned study of the interaction of α-MSH with DMPC/DMPG and DMPC/DMPA 3:1 mixtures, Table 12.1 shows the recovered values of K_p and $<\tau>_L$. The K_p values reflect the recovered blue-shifts discussed above, *i.e.*, for DMPC/DMPG a higher K_p is obtained at 37°C than at 20°C, whereas the opposite is observed for DMPC/DMPA. This interesting effect is probably related to the difference in the phase separation properties of the two lipid mixtures. At both temperatures, the DMPC/DMPG mixture is in a single phase, which is a gel phase at 20°C and a fluid phase at 37°C. A higher K_p is measured in the fluid phase, which is the usual result in one-component vesicles (Ito *et al.*, 1993). This value is similar to that measured for the DMPC/DMPA mixture at the same temperature (which is also in a single fluid phase). The interestingly increased value at 20°C for this mixture (for which there is gel/gel phase coexistence, Figure 12.1) is probably due to stronger binding of the positively charged peptide, induced by the domains enriched in anionic phospholipid.

12.3. DETERMINING THE TRANSVERSE LOCATION OF THE PEPTIDE'S FLUOROPHORE

The problem of in-depth location of the peptide using fluorescence techniques has deserved a significant attention in the fluorescence literature, and essentially addresses the location of the fluorescent amino acids Trp or Tyr. Although by now it is known that Trp is located essentially at the membrane interface, the so-called Trp anchors (de Planque *et al.*, 1999), the problem is still very relevant. The most common methodologies for obtaining topographical information are described.

12.3.1. Quenching by Lipophilic Probes

Quenching by lipophilic probes is by far the most used and perhaps the most direct methodology to obtain this type of information. Lipophilic probes which are known to be located at specific positions inside the membrane are used, and these are usually derivatized lipids or fatty acids with nitroxy-labels at specific positions along the chain (Chattopadhyay and London, 1987), or brominated lipids (Simon *et al.*, 2003). Although these are polar moieties, their location along the chain and the insertion of the chain in the phospholipid palisade structure ensure different depths in the membrane.

The data to be obtained are the Stern-Volmer plots for the fluorophore using different quenchers (a pair of quenchers is the minimum). The amount of quenching is related to the "effective quencher concentration", and this one depends on the relative positions of both quencher and fluorophore. Stern-Volmer formalisms and quenching kinetics (static or collisional mechanisms), will be described in more detail in Sub-sections 12.6.1 and 12.6.3; here a brief comment about quantitative studies on the transverse location is presented.

Studies on the quantification of the position (*e.g.*, distance to the interface), were pioneered by Chattopadhyay and London (1987) (the so-called "parallax method"). This

assumes the absence of diffusion (pure static mechanism), and a unique depth inside the bilayer is considered for both fluorophore and quencher. A two-dimensional space is used to apply a quenching sphere-of-action model. Although this is not verified in reality, as both static and dynamic contributions are present (Castanho *et al.*, 1996), and a distribution exists for both the fluorophore and quencher, this methodology has been very useful for obtaining information about the location. The model was refined by the same authors (Abrams and London, 1992), and improvements were later introduced by Ladokhin (1997). This author considers a probability of quenching which is distance dependent, and more importantly an empirical Gaussian distribution for the distance distributions. This allows the recovery of a Gaussian profile for the fluorophore, assuming distributions with equal width for all the quenchers. The present state of the art of the analysis was presented by Fernandes *et al.* (2002). These authors obtained the quencher profile distribution by Brownian dynamics and recovered both the average location and width of the fluorophore distribution.

However, in case that only more immediate information is intended, direct inspection of a Stern-Volmer plot is enough to give a mapping of the in-depth position. For this purpose there is no need to obtain time-resolved data, *i.e.*, there is no need to discriminate the eventual static and dynamic contributions. Briefly, in the situation of identical depth of probe and quencher, the Stern-Volmer constant is expectedly higher, because the "effective" or "local" quencher concentration at each membrane depth, $[Q]$, is related to the overall concentration in the membrane $[Q]_L$, via $[Q]=\beta\ [Q]_L$, where the factor β is introduced to take into account the non-homogeneous distribution of quenchers relative to the fluorophore. It should be stressed that the overall concentration of quencher in the membrane (Castanho *et al.*, 1996), should be determined taking into account the partition coefficient of the quencher (a good reference for nitroxide-labeled fatty acids is Blatt *et al.*, 1984), as well as the lipid molar volume (Marsh, 1990).

In the literature there are very good examples of quantitative approaches such as the parallax model, and thus in this review some details about the direct comparison of Stern-Volmer constants, K_{SV}, will be described. An example of this methodology to the study of membrane embedded protein segments is a structural study about those of the nicotinic acetylcholine receptor (AChR) reconstituted in asolectin vesicles (Barrantes *et al.*, 2000). For one of them, αM1, there is a cysteine (Cys) in position 222, which according to the predicted topology would be located at the centre of the membrane, because the peptide sequence is 201-IPLYFVVNVIIPC(222)LLFSFLTGLVFYLPTDSGEK-242, where the underlined sequence denotes the hydrophobic stretch of the peptide. The Cys residue was derivatized with pyrene, and a differential quenching study was carried out using 5-, 7- and 12-spin labeled fatty acids. The Stern-Volmer constants are 6.59, 1.46, and 1.14 M^{-1} respectively, clearly pointing out to a surface location of the pyrene derivative, at variance with the reported topography. The existence of three proline (Pro) residues, one of which (Pro^{221}) is adjacent to the labeled Cys, is probably the ruling factor by introducing torsions and kinks on the α-helix.

Another interesting application of the differential quenching methodology is the determination of the relative positions of the potassium channel inactivating peptide Shaker B (ShB peptide) and the non-inactivating peptide mutant (ShB-L7E) (Poveda *et al.*, 2003). The inactivating one closes the channel via the so-called "ball" mechanism, and there is in the protein a relevant negative surface potential in addition to a hydrophobic pocket. Anionic phospholipid membranes were used for carrying out this study. This peptide has no Trp residues, but the Tyr one can be used for the quenching

study. The spin labeled-fatty acids at positions 5 (5-NS) and 16 (16-NS), which are known to be located at 12 Å and 3 Å, respectively, from the bilayer centre (Chattopadhyay and London, 1987) were used.

As described above, the direct comparison of the plots can be used to obtain qualitative information about the transverse location. Interestingly, the quenching by 5-NS was small and similar for both peptides, and no definitive conclusion could be obtained about differences on the membrane topography of the two peptides. At variance, when using 16-NS a significantly higher efficiency was observed for ShB as compared to the ShB-L7E. In this way, a clearly shallower position for the latter peptide can be concluded. Interestingly, with the exception of the quenching of ShB-L7E by 16-NS, all the plots are clearly non-linear. This could eventually be due to the existence of a significant peptide fraction in water, which was non-accessible to the lipophilic quenchers used. However, from the independent determination of the partition coefficient of the peptides, it was concluded that only a very small amount (2 % for ShB and 5 % for ShB-L7E) was in this situation. In this way, the downward curvature is probably related to some complex accessibility of the quenchers to the membrane-bound peptide, as compared to the one in solution. This is a situation where a data analysis in the context of the parallax model is difficult, but even without this quantified information relevant conclusions are obtained.

However, in some cases the downward curvature can be successfully rationalized taking into account the fraction of fluorophore in water: in a study of a fragment of the gp41 ectodomain (HIV-1) in DMPG SUV (Santos *et al.*, 1998), a curvature was observed on the Trp quenching profile by 5-NS (Figure 12.5).

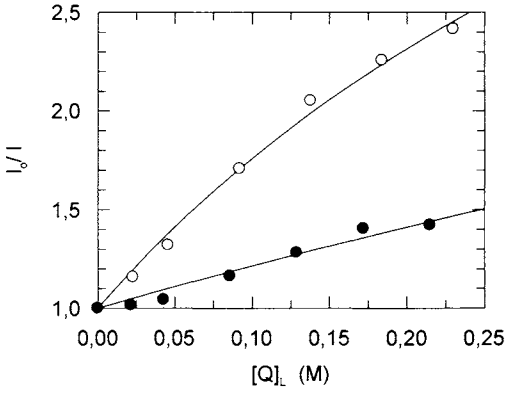

Figure 12.5. Fluorescence quenching of a fragment of the gp41 ectodomain in DMPG SUV 5.8 mM. Variation of I_o/I with the increase of the effective concentration of 5NS (O) and 16NS ( ), and fitting lines obtained using Eq. (9). Reprinted with permission from Santos *et al.* (1998). Copyright 1998 American Chemical Society.

If a typical Lehrer (1971) formalism is considered with a fraction of fluorophores accessible to the quencher contributing with a fraction f_B to the total emission, a modified Stern-Volmer plot is obtained,

$$\frac{I_o}{I} = \frac{1 + K_{SV}[Q]_L}{(1 + K_{SV}[Q]_L)(1 - f_B) + f_B} \tag{9}$$

where I_o is the fluorescence intensity in the absence of quencher, and I the fluorescence intensity in the presence of a certain quencher concentration. Data for the quenching by 5-NS could be described by Eq. (9) with $K_{SV} = 10.8 \pm 1.4$ M^{-1} and $f_B = 0.83 \pm 0.04$. This later value is in close agreement with the fraction of fluorescence intensity emitted by the peptide incorporated in the membrane at the lipid concentration used ($f_L = 0.87$), as determined from the experimental values of the partition coefficient. Therefore, all the fluorophore population in the membrane is accessible to the quencher. Data for quenching by 16-NS was also described by Eq. (9) with $K_{SV} = 2.7 \pm 0.1$ M^{-1} and the same f_B value. In this way, a surface location for this peptide can be concluded.

Sometimes, and in case that the quencher concentrations are high, static quenching contributions can be operative such as observed for the fragment 1-24 of the peptide hormone adrenocorticotropin, ACTH(1-24), in interaction with SUV of DMPC (83%) and DMPG (17%) (Moreno and Prieto, 1993). The upward curvature is described by a sphere-of-action model with a radius of 13.7 Å, which, as expected, is close to the sum of the molecular radii of Trp and quencher.

12.3.2. Quenching by Aqueous Probes

In addition to the previously described utilization of lipophilic probes, aqueous probes are also used on the study of peptide transverse location in membranes. Both acrylamide and iodide are widely used, and in most cases the Stern-Volmer constants for the peptide in interaction with the membrane is compared to the value obtained in water. In case that the peptide is shielded, *i.e.*, internalized and not adsorbed at the membrane surface, the K_{SV} value decreases. This approach is not as informative as the methodology previously described based on lipophilic quenchers located at a graded series of depths in the membrane.

One interesting example of acrylamide quenching, involves again the peptide ACTH (1-24) introduced in the previous sub-section and a related peptide. In this case, the quenching data, shown in Figure 12.6, presents a downward curvature in both cases. This data could be described by a model (Eq. 10) taking into account the peptide fluorescence arising from the fraction in water (f_w), as well as two other fractions in the lipid, one accessible (f_{La}) and another not accessible to the quencher (f_{Ln}):

$$\frac{I_o}{I} = 1 \Big/ \left(\frac{f_W}{1 + K_{SV}^W[Q]} + \frac{f_{La}}{1 + K_{SV}^L[Q]} + f_{Lb} \right) \tag{10}$$

The value of K_{SV}^W is known from an independent study in aqueous solution, and f_w is easily calculated from the peptide partition coefficient since the lipid concentration is known. In this way, K_{SV}^L, f_{La} and f_{Ln} can be obtained from the fitting. It should be stressed that a model with just two populations (in water and in the membrane) could not describe the data. This experiment clearly shows that there is some internalization of Trp, but no precise information about the transverse location is obtained. This is only obtained via the

nitroxide fatty acid quenching study, which showed that in fact the peptide is located near the surface although shielded from acrylamide.

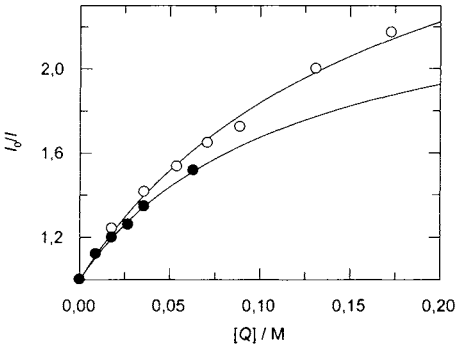

Figure 12.6. ACTH(1-24) (closed circles) and related peptide (open circles) fluorescence quenching by acrylamide in the presence of 2mM DMPC/DMPG (83:17) SUV. The lines are the fits of Eq. (10) to those data series. Adapted from Moreno and Prieto (1993).

12.3.3. Resonance Energy Transfer

The energy transfer efficiency is explicitly dependent on the inverse sixth power of the distance between donor and acceptor. This very important methodology will be dealt with in more detail later in this work, when addressing the problem of peptide aggregation in the membrane, but here its application on the determination of the peptide in-depth location in the membrane will be presented. This approach is similar to the above described methodology using lipophilic quenchers, *e.g.*, acceptors located at a graded series of depths can be used to report on proximity, but in this case it is not a contact (either collisional or static), but a dipolar interaction. Trp and Tyr are usually used as donors, as their fluorescence emission occurs at short wavelengths.

An example of this type of application is the location of Trp in the hormone ACTH (1-24) (Moreno and Prieto, 1993). In this case, derivatized fatty-acids with the anthroyl chromophore were used as acceptors (3-AS and 12-AS). It should be stressed that in addition to the above described spin labeled fatty-acids, this is the best characterized family of probes for this type of studies (Blatt *et al.*, 1984; Villalaín and Prieto, 1991). The Förster radius (Eq. (26) in Sub-section 12.6.2) for the Trp/3-AS and the Trp/12-AS pairs is R_0= 24 Å (the same value for both pairs is due to the identical absorption spectra of both acceptors). Similar efficiencies were determined with both probes, which means that the interplanar donor-acceptor distance (Davenport *et al.* 1985) was identical in both cases, *i.e.*, Trp is located in the membrane in-between the 3- and the 12-AS probes. In this way it is not deeply buried, but neither is adsorbed near the interface.

In another work, the above described study of the inactivating peptide ShB of the potassium channel and the non-inactivating mutant ShB-L7E (Poveda *et al.*, 2003) in interaction with membranes, FRET from the Tyr residue of these peptides to *t*-PnA was used. The acceptor, *t*-PnA, is known to be internalized in the membrane (Castanho *et al.*, 1996), with the tetraene chromophore centered at a distance of 12.1 Å from the interface

(de Almeida *et al.*, 2002). The Förster radii for these systems are $R_0 = 25.8 \pm 0.2$ Å (ShB) and $R_0 = 26.4 \pm 0.2$ Å (ShB-L7E). In Figure 12.7, the variation of the energy transfer efficiency *vs.* the number of acceptor per R_0^2 is shown. FRET is more efficient from ShB as compared to that from ShB-7LE, and therefore the former peptide is more deeply located in the membrane as compared to the latter. In addition, in Figure 12.7 is also presented the theoretical expectation for energy transfer in two-dimensions and a good agreement is found for the ShB/*t*-PnA pair. Since this curve was derived assuming no interplanar separation, this experiment locates precisely the depth of Tyr inside the membrane, such as could be concluded from the "parallax model". For the ShB-7LE, an interplanar separation of 12 Å describes the data, so this peptide's fluorophore is clearly near the surface (for more details in interplanar FRET see Section 12.7).

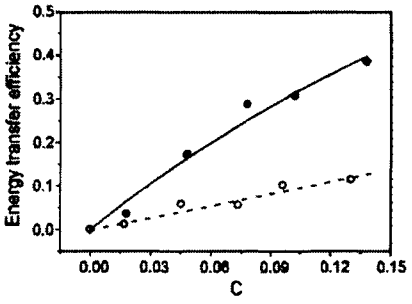

Figure 12.8. FRET efficiency between ShB peptide (closed circles) or mutant ShB-L7E peptide (open circles) and *t*-PnA as a function of C, the number of acceptor molecules per R_0^2. The solid line is the theoretical expectation for bidimensional random distribution of acceptors (in-plane FRET), and the dotted line is just a guide to the eye. Reprinted with permission from Poveda *et al.* (2003). Copyright 2003 American Chemical Society.

12.3.4. Emission Spectra of Tryptophan and Tyrosine, and Red-Edge Excitation Shift

One of the most immediate information about the fluorophore environment comes from its spectral distribution. Trp emission maximum undergoes a significant red-shift from a non-polar (~320 nm) to a solvating environment (~350 nm), and this has been used to follow, *e.g.*, protein denaturation. However, the membrane interface is a complex anisotropic medium, and from the blue-shift of Trp upon interaction with the membrane, it is not possible to obtain quantitative information about in-depth location.

Red-edge excitation shift (REES) is a very interesting phenomenon which was pioneered among others by Weber (Weber and Shinitzky, 1970; Valeur and Weber, 1977), and can be used in biophysics for obtaining topographical information (for a review see Chattopadhyay, 2003). This effect, *i.e.*, an increase of the maximum emission wavelength of fluorescence upon exciting on the tail of the absorption band, with a concomitant increase in anisotropy, is observed for fluorophores in a polar and motion-restricted environment. The effect is related to a dipole relaxation occurring on the time scale of fluorescence emission. The interfacial region of membranes is characterized by these properties, so if a strong effect is observed, it points to a surface location since the

membrane core is non-polar and less rigid. We obtained for a peptide in interaction with a membrane (Santos *et al.*, 1998) an impressive REES of 18 nm which is a clear evidence of an interfacial location. However, as compared to the differential quenching methodology, no precise quantitative information can be obtained.

12.4. OBTAINING INFORMATION ON THE SECONDARY STRUCTURE OF THE PEPTIDE FROM FLUORESCENCE INTENSITY DECAYS

As previously described, Trp fluorescence emission decay kinetics is usually complex, and in addition to a sum of exponentials, continuous distributions of lifetime populations have also been used to describe the fluorescence decays (*e.g.* Vincent *et al.*, 2000). In fact, the lifetime of Trp can be influenced by a wide variety of factors that include solvent quenching, quenching by groups in the protein itself and electron transfer to the carbonyl of the peptide bond (Engelborghs, 2001). The complexity of single Trp peptides and proteins fluorescence decay kinetics can arise from two different but not mutually exclusive phenomena, namely the existence of ground state heterogeneity, usually attributed to different rotamers (*e.g.*, Willis and Szabo, 1992) and solvent relaxation processes (Lakowicz, 2000; Toptygin *et al.*, 2001). Multi-exponential decay in single Trp proteins has also been described as originating from the internal motion of Trp in the proteins, due to a coupling of internal motion and angle (and possibly distance) dependent quenching efficiency of neighboring quenchers (Tanaka *et al.*, 1994) and from reversible excited state dynamics (Engelborghs, 2001). This complexity intrinsic to Trp emission decays precludes its utilization in the recovery of direct information about, *e.g.*, secondary structure in peptides/proteins (Ladokhin, 2001). However, structural information can still be recovered from time-resolved fluorescence data of Trp residues as illustrated in the following study of the interaction of α-MSH with negatively charged vesicles, for which partition, emission shift and residual anisotropy results were presented in the previous section.

The primary structure of α-MSH is Ac-Ser-Tyr-Ser-Met-Glu-His-Phe-Arg-Trp-Gly-Lys-Pro-Val-NH_2. It appears that the peptide has no preferred structure in water (Biaggi *et al.*, 1997), being very flexible, whereas all its synthetic analogs with superpotent biological activity present a β-turn (or sometimes another kind of turn) stabilized within their central region comprising residues 6-9, *i.e.*, His-Phe-Arg-Trp (Sawyer *et al.*, 1980, 1982; Al-Obeidi *et al.*, 1989). This Trp-containing region of the peptide is furthermore the minimum melanotropic message sequence, essential for ligand binding and biological function (Hruby *et al.*, 1987).

The α-MSH tryptophanyl fluorescence decay in buffer is complex (described by three exponentials), and from the fits, a short component (τ_1= 0.448 ns (20°C) or 0.307 ns (37°C); a_1 = 0.18), an intermediate component (τ_2= 2.00 ns (20°C) or 1.36 ns (37°C); a_2 = 0.48) and a long component (τ_3= 3.45 ns (20°C) or 2.35 ns (37°C); a_3 = 0.34) are obtained. In the presence of both lipid systems at the two temperatures studied a variation of both the lifetimes and amplitudes of the components is observed. The data for the DMPC/DMPA (3:1) mixture at 20°C is depicted in Figure 12.8, and the trend of variation is similar to the one obtained for the DMPC/DMPG mixture. The short lifetime is essentially invariant while the intermediate one increases slightly and reaches a plateau and a marked increase is observed for the long one which varies from 3.45 ns in buffer up

to 6.72 ns for the highest lipid concentration. Regarding the amplitudes, that of the short component shows a very slight increase; the amplitude of the intermediate component increases significantly and for the amplitude of the long one a correspondent decrease is obtained, both reaching a plateau at higher lipid concentrations. The amplitudes and the lifetimes of the components in aqueous solution are similar to those obtained by Ito *et al.* (1993).

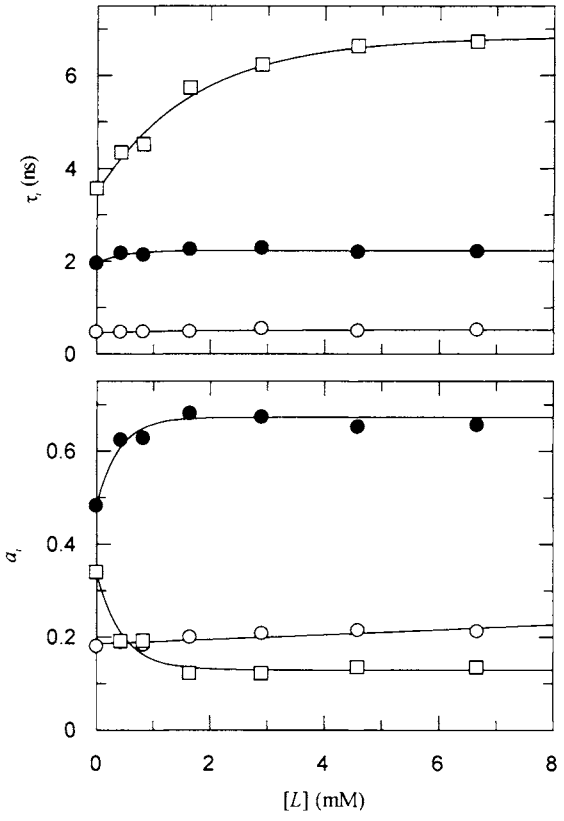

Figure 12.8. Fluorescence lifetime components τ_i and respective normalized pre-exponentials a_i for α-MSH (λ_{exc}= 295 nm, λ_{em} = 350 nm) *vs.* lipid concentration [*L*] (DMPC/DMPA (3:1) LUV) at 20°C. The solid lines are merely guides to the eye and have no physical meaning. Reprinted with permission from Contreras *et al.* (2001). Copyright 2001 Biophysical Society.

The lifetime-weighted quantum yield, $<\tau>$ (Eq. 5), of α-MSH in water at 20°C is very close to the value for Trp in aqueous solution at the same temperature ($<\tau>$ = 2.25 ns) (Lakowicz, 1999) and just slightly higher than the value for α-MSH reported in the literature ($<\tau>$ = 2.09 ns) (Ito *et al.*, 1993). If we extrapolate the values at different temperatures reported in that work, the fluorescence lifetime at 37°C ($<\tau>$ = 1.51 ns) is in very good agreement with our data.

From the partition coefficient study previously described (Eq. 6), $\langle\tau\rangle_L$, the lifetime-weighted quantum yield of the peptide interacting with the membrane was determined and the values for the two membrane model systems are presented in Table 12.1. The values are longer in the DMPC/DMPG vesicles as compared to the DMPC/DMPA ones at the same temperature.

Upon interaction with the lipid system, the peptide undergoes alterations of its secondary structure and these can be appreciated from the trend of variation of both lifetime components and pre-exponentials (Figure 12.8). It is difficult to infer about the secondary structure of the peptide from the fluorescence decays in the different environments mainly because there are still very few studies made on peptides in which the Trp residue is in a position of known structure, and Dahms and Szabo (1995) point to subtleties that require caution when predicting structures. However, from the trend of variation of the time-resolved data, it can be concluded that upon membrane incorporation, α-MSH undergoes strong structural changes, which is in agreement with the IR data (Contreras *et al.*, 2001). However, it should be stressed that this pattern of fluorescence time-resolved data only reports the peptide structure in the vicinity of the Trp residue, whereas global information about all the peptide structure is obtained from IR. Thus, there is no contradiction when the very same pattern of variation was obtained for both lipids, at variance with IR data which allowed concluding that intermolecular aggregates are the dominant structural feature in DMPG-containing vesicles, while in DMPA-containing vesicles some random structure is present.

The structural information obtained for the α-MSH peptide was possible to obtain because there was a "reference state" (the decay in buffer, where the peptide has a random structure). In fact, it is only possible to extract reliable information on the Trp vicinity of peptides and proteins when a comparison can be made (Engelborghs, 2001). The trend displayed by the lifetimes and amplitudes of the decay components can be appreciated as a function of lipid concentration, as shown here or, *e.g.*, in the absence *vs.* presence of (varying concentrations of) a denaturing agent (Dahms and Szabo, 1995).

The multi-exponential behavior of single Tyr peptides and proteins has been extensively reported, and has been attributed to the existence of ground state rotamers sensing different chemical environments and interconverting slowly on the nanosecond timescale (Laws *et al.*, 1986), and thus the fluorescence decay of those peptides and proteins should, in principle, contain some structural information.

12.5. FLUORESCENCE ANISOTROPY OF THE PEPTIDE CONTAINS STRUCTURAL AND DYNAMICAL INFORMATION

Depolarization of the fluorophore emission can occur through a variety of processes. In the absence of phenomena such as energy homotransfer (see sub-section 12.6.5), the rotational dynamics of the fluorophore is the determinant factor. This dynamics depends on parameters that include temperature, the viscosity of the surrounding medium, and the size and shape of the molecule containing the fluorophore. Consequently, important structural and dynamical information can be extracted from anisotropy measurements, both time-resolved and to a lesser extent, steady-state.

The anisotropy decays of fluorophores in biomolecules are usually complex, as several movements contribute to the depolarization process. They are usually described by a sum of exponentials,

$$r(t) = (r_0 - r_\infty)\sum_i \beta_i \exp(-t/\varphi_i) + r_\infty \tag{11}$$

where r_0 is the fundamental anisotropy (at time zero, and depends only on the fluorophore), φ_i are the rotational correlation times, β_i their respective amplitudes ($\Sigma\ \beta_i = 1$), and r_∞ the residual or limiting anisotropy. The anisotropy decay parameters are obtained using a nonlinear least-squares global analysis method by simultaneously fitting the vertically and horizontally polarized emission components of the decay to Eq. (11). The steady-state anisotropy in turn, is obtained from the steady-state intensity components (Jabłoński, 1960):

$$< r >= (I_{VV} - GI_{VH})/(I_{VV} + 2GI_{VH}) \tag{12}$$

where the different intensities I_{ij} are the steady-state vertical and horizontal components of the fluorescence emission with excitation vertical (I_{VV} and I_{VH}, respectively) and horizontal (I_{HV} and I_{HH}, respectively) to the emission axis. The latter pair of components is used to calculate the G factor ($G = I_{HV}/I_{HH}$; Chen and Bowman, 1965).

In the case of the aforementioned α-MSH, the steady-state anisotropy in water has a very low value, both at 20°C ($<r>$ = 0.0144 ± 0.0003) and at 37°C ($<r>$ = 0.0146 ± 0.0007). The time-resolved anisotropy decays to zero, with a single rotational correlation time of 0.52 ± 0.02 ns and 0.32 ± 0.01ns, respectively. Sub-nanosecond φ values, and absence of a limiting anisotropy, justify the low values of the steady-state anisotropy. In fact, for molecules with a single rotational correlation time and complex fluorescence intensity decay, the steady-state anisotropy is given by the following composition of Perrin (1926, 1929) equations (based on the law of anisotropy addition; Weber, 1960):

$$< r >= \frac{r_0 - r_\infty}{< \tau >} \sum_i \frac{a_i}{1/\tau_i + 1/\varphi} + r_\infty \tag{13}$$

which leads to values of $<r>$ coincident with the experimental steady-state values. The rotational correlation time can alternatively be calculated assuming spherical geometry for the peptide. In this case, $\varphi = \eta V/RT$ where η is the viscosity of the solvent, and V the volume of the rotating unity. The volume of the peptide can be estimated to be 1821 Å^3 (Zamyatnin, 1972) and in this case the values predicted are φ = 0.45 ns (20°C) and φ = 0.29 ns, which are only slightly shorter than the experimental ones. Thus, we can conclude that the peptide is essentially monomeric in aqueous solution for the concentrations used in fluorescence measurements (~30 μM), whereas IR spectra, carried out on more concentrated samples indicate the presence of peptide aggregates at those temperatures (Contreras *et al.*, 2001).

When in the presence of lipid bilayers, a positive limiting anisotropy is reached, as described in Section 12.2. In this case, even in the presence of a high lipid concentration, the fraction of peptide remaining in the aqueous phase can contribute significantly to the

fluorescence emission of a sample. This implies that a detailed analysis of the fluorescence anisotropy decay of the peptide at shorter times is eventually too complex, because the fitting model would have to consider at least two different peptide populations, each associated with a complex fluorescence intensity decay. However, the study of limiting anisotropies of the peptide in the membrane is not hampered by this fact, and in Section 12.2 it was shown how to obtain the value of r_∞ for the peptide interacting with the membrane. From the values give in Table 12.1, it can be seen that the limiting anisotropies obtained are in all cases very high, considering that the fluorophore is not a typical hydrophobic molecule incorporated into the membrane core. This means that the peptide is strongly adsorbed at the membrane/water and the wobbling motion of Trp is very restricted, even in the fluid phase. Irrespective of the structure adopted by the peptide in the vesicles, not only it is thermally stabilized (see previous section) but it is also very rigid. The limiting anisotropies are related to the order parameter, S, describing the equilibrium orientation distribution of the probe at times much larger than the rotational correlation time, and the fundamental anisotropy r_0, through the following relationship (Best *et al.*, 1987):

$$S^2 = \frac{r_\infty}{r_0} = \left\langle \frac{3\cos^2\theta - 1}{2} \right\rangle^2 \tag{14}$$

where θ is the angular rotation of the emission transition moment and the angle brackets indicate an average over the entire fluorophore population, assuming cylindrical symmetry. If we consider a fundamental anisotropy for Trp excitation at 295 nm of r_0 = 0.24 (Valeur and Weber, 1977) an angle $\theta = 25°$ is obtained for the gel phase, or θ = 27-31° for the fluid phase. In a molecular dynamics study by Pascutti *et al.* (1999), the peptide acquired, in a low dielectric constant medium, a packed conformation that remained stabilized for more than 7.0 ns of the simulation, and as already mentioned, the superpotent analogs possess a stabilized turn involving the Trp residue (Sawyer *et al.*, 1982). Based on the results presented here, it is reasonable to predict that the interaction of α-MSH with negatively-charged membranes induces and stabilizes a specific conformation, probably involving the Trp-containing message region, which could be similar to the one found for the superpotent analogs, and therefore necessary for its biological activity.

A more detailed study could be performed with the shaker B (ShB) peptide, because due to its higher partition coefficient it is possible to have a very low fraction of peptide in the aqueous phase in the presence of relatively low lipid concentrations (Poveda *et al.*, 2003). The ShB peptide comprises the 20 N-terminal amino acids (H_2N-MAAVAGLYGLGEDRQHRKKQ) of each subunit in the Shaker B potassium channel, the so called inactivating "ball" responsible for inducing fast, N-type inactivation in this and many other related or unrelated channels (*e.g.*, Hoshi *et al.*, 1990). Previous biophysical studies with a fluorophore-labeled ShB peptide suggested that the peptide binds to lipid vesicles with high affinity, readily adopts a strongly hydrogen-bonded intramolecular β-hairpin structure and becomes inserted into the hydrophobic bilayer in a monomeric form. In contrast, the non-inactivating mutant ShB-L7E also binds phospholipids vesicles, but is unable to either form the characteristic β-structure or get into the hydrophobic core of the bilayer. ShB peptide contains a single Tyr residue and no

Trp. Tyr displays a high intrinsic anisotropy and a fluorescence lifetime optimal to characterize nanosecond and sub-nanosecond motions in peptides and proteins (Ferreira *et al.*, 1994).

The steady-state fluorescence anisotropy measured in buffer at 22°C by exciting at 285 nm was relatively similar for both peptides ($\langle r \rangle$ = 0.039 and $\langle r \rangle$ = 0.051 for ShB and ShB-L7E, respectively) and much smaller than the fundamental anisotropy (r_0 = 0.29) corresponding to immobilized Tyr at that excitation wavelength (Gryczynski *et al.*, 1991).

Table 12.2. Time-resolved fluorescence parameters of ShB and ShB-L7E (rotational correlation times, φ_i, amplitudes, β_i, and residual anisotropy, r_∞) in aqueous buffer and incorporated into PA vesicles at 22°C.

Peptide	Medium	r_0	β_1	φ_1 (ns)	β_2	φ_2 (ns)	r_∞	χ^2
ShB	Buffer	0.20	0.51	0.2	0.49	0.9	0	1.0
ShB-L7E	Buffer	0.20	0.67	0.2	0.33	0.9	0	1.0
ShB	PA	0.17	0.42	0.2	0.58	4.3	0.07	1.0
ShB-L7E	PA	0.18	0.64	0.1	0.36	0.3	0.06	1.1

Reprinted with permission from Poveda *et al.* (2003). Copyright 2003 American Chemical Society.

In the time-resolved anisotropy experiments, two rotational correlation times were needed to describe the decay processes, which were similar for both peptides (Table 12.2). Since the long rotational correlation time (φ_2) was five times longer than the short one (φ_1), the total anisotropy can be interpreted as the product of two independent depolarizing processes, a first one due to fast movements of the peptide segment containing the Tyr residue [$r'(t)$], and a second one related to the global motion of the whole peptide (Lipari and Szabo, 1980):

$$r(t) = r'(t)\exp\left[\left(1 - S_2^2\right)\exp\left(-t/\varphi_{global}\right) + S_2^2\right]$$
$$r'(t) = r(0)\left[\left(1 - S_1^2\right)\exp\left(-t/\varphi_{segmental}\right) + S_1^2\right] \quad (15)$$

where S_1 and S_2 are the order parameters characterizing the internal and the whole peptide fluctuations. The anisotropy decays to zero for both peptides in buffer, thus in this case S_2 = 0. The short and long rotational correlation times obtained from the fit are related to φ_{global} and $\varphi_{segmental}$ (Table 12.3) by

$$\varphi_2 = \varphi_{segmental}$$
$$\varphi_1 = \left(\varphi_{segmental}\varphi_{global}\right)/\left(\varphi_{segmental} + \varphi_{global}\right) \quad (16)$$

The longest rotational correlation time, similar for both peptides, reflecting the motion of the whole peptide, can be used to estimate the equivalent hydrodynamic radius

R, assuming spherical symmetry. From $\varphi = \eta V/RT$, and as $V = 4\pi R_h^3$, a value of $R_h = 9.6$ Å is computed. By independent methods the radius is estimated to be 9.4 Å, and thus the peptide is essentially monomeric (Poveda *et al.*, 2003). The segmental rotational correlation time is restricted, as shown by the S_1 values in Table 12.3. Assuming a "wobbling in cone" model in which the molecule exists in a square-well potential beyond which further angular displacement is energetically impossible, the angular displacement can be calculated from S_1 (note that this is a different principle than the one that leads to Eq. (14)), through the relationship (Kinosita *et al.*, 1982):

$$S_i = \frac{\cos^2\theta + \cos\theta}{2} \tag{17}$$

(or equivalently, $\cos\theta = \frac{1}{2}[(8S_i+1)^{1/2} - 1]$). The restriction is more severe in ShB (angular displacement of 38°), as compared to ShB-L7E (47°). The steady-state anisotropy of both peptides showed a large increase upon addition of egg PA vesicles, and from a fit of Eq. (3) the partition coefficient and the steady-state anisotropy values for both peptides incorporated in the membrane were determined ($K_p = (4.5 \pm 0.5) \times 10^4$, $\langle r \rangle = 0.120 \pm 0.003$ for ShB and $K_p = (2.2 \pm 0.3) \times 10^4$, $\langle r \rangle = 0.093 \pm 0.003$ for ShB-L7E). The partition coefficients are much higher than those previously presented for α-MSH.

Table 12.3. Parameters from the fit of an independent two-motion model to the anisotropy decay of ShB and SHB-L7E (segmental and global correlation times, φ_i, order parameters, S_i, and cone angles, θ_{0i}) in aqueous buffer and incorporated into PA vesicles at 22°C.

Peptide	Medium	$\varphi_{segmental}$ (ns)	φ_{global} (ns)	S_1	S_2	θ_{01} (deg)	θ_{02} (deg)
ShB	Buffer	0.2	0.9	0.70	0	38	
ShB-L7E	Buffer	0.2	0.9	0.57	0	47	
ShB	PA	0.1	4.3	0.87	0.75	24	35

The fluorescence anisotropy decays for the peptides ShB and ShB-L7E have very different kinetics, but in both cases a residual, time-independent value different from zero is reached (Figure 12.9), indicating a restricted motion of the Tyr side chain on the timescale of the fluorescence emission. The fitting parameters are shown in Table 12.2. Two rotational correlation times were needed to describe the decay processes. In the case of the mutated peptide, they were both very short, whereas for the ShB peptide, the shorter one was identical to the one in buffer, but the long one was much higher.

The two rotational correlation times for ShB differ by more than a order of magnitude, and again, they can be attributed to two independent molecular motions. Following the model previously used for aqueous solution, and applying Eq. (15, 16), the order parameters and the values of $\varphi_{segmental}$ and φ_{global} can be obtained (Table 12.3).

Quenching and FRET experiments show that the Tyr residue of ShB peptide is located much deeper into the membrane than that of ShB-7LE (Sub-sections 12.3.1 and 12.3.3). All the above mentioned results agree with the burying of the β-hairpin of ShB

into the hydrophobic region, parallel to the phospholipids acyl chains. An additional C-terminal portion would remain lying over the membrane surface facilitating electrostatic interactions. According to this model, at least two rotational correlation times and a residual anisotropy must be extracted from the time-resolved anisotropy experiments of the ShB peptide inserted in membranes: a short correlation time which reflects internal fluctuations of the Tyr residue, a longer component corresponding to fluctuations of the whole peptide segment incorporated into the membrane, and a residual value which shows that the reorientation motion of the Tyr side chain is restricted on the timescale of the fluorescence emission due to interactions with phospholipid chains.

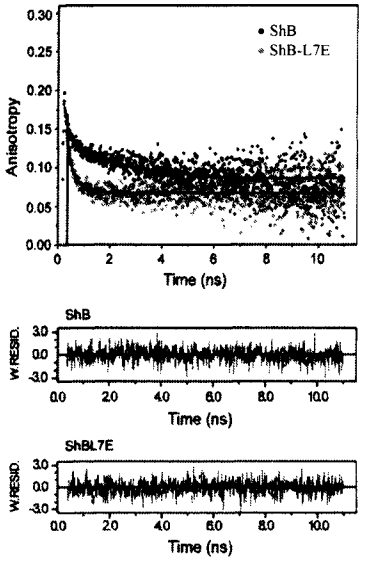

Figure 12.9. Time-resolved fluorescence anisotropy of the Tyr residue of the ShB and the mutant ShB-L7E peptides in PA LUV at 22°C. Experimental data and that from the corresponding fit (see Table 12.2 for decay parameters) are shown as points and as a continuous line, respectively. Residuals of each fit are also shown. Excitation and emission wavelengths were 285 and 320 nm, respectively. Reprinted with permission from Poveda *et al.* (2003). Copyright 2003 American Chemical Society.

Assuming that the hairpin structure behaves like a rigid body into the bilayer, we could estimate the diffusion coefficient corresponding to the rigid body fluctuations from the longest rotational correlation time as $D_{\perp} = \sigma/\varphi_{global}$ (Kinosita *et al.*, 1982; Vogel *et al.*, 1988) where σ is a function of the order parameter S_2 and can be computed from the polynomial approximation described by Mateo *et al.* (1996). Modeling the hairpin as a cylinder with a diameter of 8 Å and assuming a lipid viscosity of *ca.* 0.2 P (Best *et al.*, 1987) a volume of $\approx$ 850 Å^3 was estimated, which is in agreement with the volume of the N-terminal 1-10 amino acids in ShB, corresponding to the hydrophobic half of the peptide. The β-turn would be formed by the sequence 4-7 (VAGL) establishing four stabilizing intramolecular hydrogen bonds. The glycine residue at position 11, due to its larger degree of rotational freedom, could act as a hinge, allowing the fluctuations of the

membrane embedded sequence. In this way, it is useful to calculate the amplitude of these fluctuations, which can be obtained from the order parameter S_2, assuming the wobbling in a cone model (Eq. 17). An angular displacement of 35° was obtained, which is smaller than the value reported in fluid membranes from electron paramagnetic resonance and fluorescence depolarization techniques for anchored rigid probes (for a review, see Mateo *et al.*, 1996) and helical polypeptides containing Trp (Vogel *et al.*, 1988). The small angle suggests that the restriction in the motion of the β-hairpin structure is due not only to the phospholipid chains but also to intramolecular interactions with adjacent residues and to the strong electrostatic interactions established between the C-terminal portion of the peptide and the bilayer surface. Furthermore, the short correlation time for the membrane-bound form is similar to the one obtained in buffer, but the angular displacement of this motion is smaller (24° *vs.* 38°), and indicates that the hydrogen-bonded structure adopted by the peptide in the bilayer, together with the proximity of the phospholipids acyl chains, restrict strongly the amplitude of the motion in the Tyr-containing peptide segment.

Finally, the dynamics of ShB-L7E in the membrane is very different from that of ShB, exhibiting two short rotational correlation times. These could correspond to rotational motions of short segments in a fluid medium. The limiting anisotropy value also indicates that the amplitude of these motions is restricted. If we consider that the peptide lies at the membrane surface interacting electrostatically with the phospholipid head groups, the global rotational motion of the peptide is then prevented, and only rapid albeit constrained fluctuations of the Tyr side chain can take place, in agreement with the parameters recovered from the anisotropy decays.

In sum, our results show that a wide variety of molecular details regarding the ShB *vs.* the ShBL7E peptide interaction with membranes can be obtained using the intrinsic fluorescence of their single Tyr residue.

12.6. FORMATION OF PEPTIDE-RICH PATCHES/PEPTIDE AGGREGATES *VS.* RANDOM DISTRIBUTION

The peptide fluorescence, either from Trp or Tyr residue(s), or a covalently-labeled probe, can be highly dependent on its aggregation state. For instance, if there is the possibility of self-quenching, the oligomerization of the peptide, leading to stable aggregates, can result in a static quenching process. On another hand, the formation of peptide rich domains without stable aggregates can lead to an increased dynamic self-quenching, due to the fact that the local concentration of peptide is higher than that expected on the basis of a random distribution on the whole bilayer. The situations of static and dynamic quenching can be easily distinguished if both steady-state and time resolved measurements are performed. Additionally, FRET, due to its strong distance-dependence, is also very useful addressing these questions.

12.6.1. Aggregation State and Lateral Distribution of M13 Major Coat Protein from Self-Quenching Studies

M13 major coat protein is the main protein component of the filamentous bacteriophage M13, with about 2800 copies. It contains a single hydrophobic

transmembrane segment of approximately 20 amino acid residues, apart from an amphipathic N-terminal arm and a heavily basic C-terminus with a high density of lysine (Lys) residues (for reviews see Stopar *et al.*, 2003; Hemminga *et al.*, 1993). It has been known to exist in many aggregation states, depending on factors like isolation, reconstitution procedure, pH, ionic strength, and amphiphile composition (Hemminga *et al.*, 1993; Stopar *et al.*, 1997). The mechanism of phage assembly in the *Escherichia coli* membrane is not yet completely understood, but the assembly site is thought to be composed of a dynamic protein-lipid network, characterized by the absence of a preferential association between M13 coat protein and/or lipids (Hemminga *et al.*, 1993), which allows storage of monomeric coat protein at very high local concentrations, as the insertion of the protein in the assembling phage particle is only possible on the monomeric form (Russel, 1991). The type of interactions between lipids and coat protein that allows the formation of this structure is largely unknown. It has been proposed that the self-association behavior of transmembrane proteins incorporated in lipid membranes is influenced by hydrophobic matching conditions on the protein-lipid interface (Mouritsen and Bloom, 1984; Killian, 1998). The monomeric protein is expected to be stable under perfect matching conditions with the surrounding phospholipid milieu. In case of hydrophobic mismatch at the protein-lipid interface, it is possible that the boundary lipids reorganize themselves, to lower the tension created by exposure of hydrophobic acyl chains or amino-acid residues, which can be achieved by ordering/disordering of the phospholipids (Nezil and Bloom, 1992). Moreover, if the hydrophobic mismatch is too high for correction with small adjustments of bilayer hydrophobic thickness, this might result in protein aggregation to obtain minimization of the protein-lipid contacts (Ren *et al.*, 1999; Lewis and Engelman, 1983; Mobashery *et al.*, 1997; Mall *et al.*, 2001).

In order to obtain information on the influence of lipid bilayer composition on the lateral distribution and oligomerization properties of M13 coat protein in membrane model systems, several fluorescence methodologies (fluorescence self-quenching, absorption and emission spectra, and energy transfer) were applied (Fernandes *et al.*, 2003), using the protein derivatized with n-(4,4-difluoro-5,7-dimethyl-4-bora-3a,4a-diaza-s-indacene-3-yl)methyl iodoacetamide (BODIPY FL C_1-IA) or n-(iodoacetyl)aminoethyl-1-sulfonaphthylamine (IAEDANS). The fluorescence decay of BODIPY in the labeled mutant proteins incorporated in 1,2-dioleoyl-*sn*-glycero-3-phosphocholine (DOPC; C18:1 acyl chains), 1,2-dimyristoleoyl-*sn*-glycero-3-phosphocholine (DMoPC; C14:1 acyl chains)/DOPC, 1,2-dierucoyl-*sn*-glycero-3-phosphocholine (DEuPC; C22:1 acyl chains)/DOPC, DMoPC, and DEuPC bilayers was described by two components, $\tau_1 = 6.23$ ns ($a_1 = 0.90$) and $\tau_2 = 3.27$ ns, which leads to an average lifetime, calculated by (*e.g.*, Sillen and Engelborghs, 1998):

$$\bar{\tau} = \sum_i a_i \tau_i^2 \Big/ \sum_i a_i \tau_i \tag{18}$$

of $\bar{\tau} = 6.1$ ns, as measured in samples with $[\text{BD-M13 coat protein}]_{\text{eff}} < 10^{-3}$ M (BODIPY-labeled protein effective membrane concentration). For the determination of protein effective concentration in the membranes, the lipid molar volumes were calculated from the reported lipid area (72 Å^2) and membrane thicknesses (Tristam-Nagle

et al., 1998; Lewis and Engelman, 1983). From the fluorescence lifetimes, the dynamical contribution for quenching can be discriminated.

The effects of the collisional contribution of self-quenching on the fluorescence lifetime for a molecule with a complex decay are described by the Stern-Volmer equation (Sillen and Engelborghs, 1998):

$$<\tau>_0/<\tau> = 1 + <k_q> . \bar{\tau}_0 [F] \tag{19}$$

The subscript 0 indicates the absence of quencher (in our case, the values for the sample with the lowest protein concentration), $<k_q>$ is the bimolecular quenching rate constant, the brackets indicate that this is a (complex) average of the rate constants related to each component of the decay, and $[F]$ is the concentration of the fluorophore. By increasing effective protein concentration, and considering a random protein distribution in the bilayers, linear self-quenching Stern-Volmer plots are obtained (Fernandes *et al.*, 2003) and $<k_q>$ values are recovered (Table 12.4).

Table 12.4. Bimolecular diffusion rate constants, $<k_q>$, diffusion coefficients, D, and apparent sphere-of-action radii (R_S) recovered from BODIPY fluorescence emission self-quenching from BODIPY-labeled T36C and A35C mutants of M13 major coat protein.

Systems	$< k_q > / (10^9\ M^{-1}s^{-1})$	$D / (10^{-7}\ cm^2s^{-1})$	R_s (Å)
T36C in DOPC	2.3	0.7	14
A35C in DOPC	1.7	0.4	14
A35C in DMoPC	2.6	0.8	23
A35C in DEuPC	5.0	2.6	27
T36C in DMoPC/DOPC	6.6	4.2	14
T36C in DEuPC/DOPC	20	22	14

Reprinted from Fernandes *et al.*, (2003) with permission. Copyright 2003 Biophysical Society.

In the analysis of the steady-state fluorescence intensities, the static quenching (described by the sphere-of-action model) has to be taken into account. The combined contributions of the collisional and the sphere-of-action effects on the fluorescence intensity are given by Loura *et al.* (2000) as

$$I_F = \frac{C \times [F]}{1/\tau_0 + < k_q > [F]} \exp(-V_s N_A [F]) \tag{20}$$

Here, I_F is the fluorescence intensity, C is a constant, and V_s is the sphere-of-action volume, from which the sphere-of-action radius is obtained. In the absence of protein aggregation this radius should be close to the sum of the van der Waals radii. Eq. (20) was used to analyze the fluorescence steady-state quenching profiles for BD-M13 coat

protein in DOPC, DMoPC/DOPC, DEuPC/DOPC, DMoPC, and DEuPC (Figure 12.10). Because $<k_q>$ values were obtained from the lifetime quenching profile, the fluorescence quenching contribution of the sphere-of-action effect could be retrieved (Table 12.4).

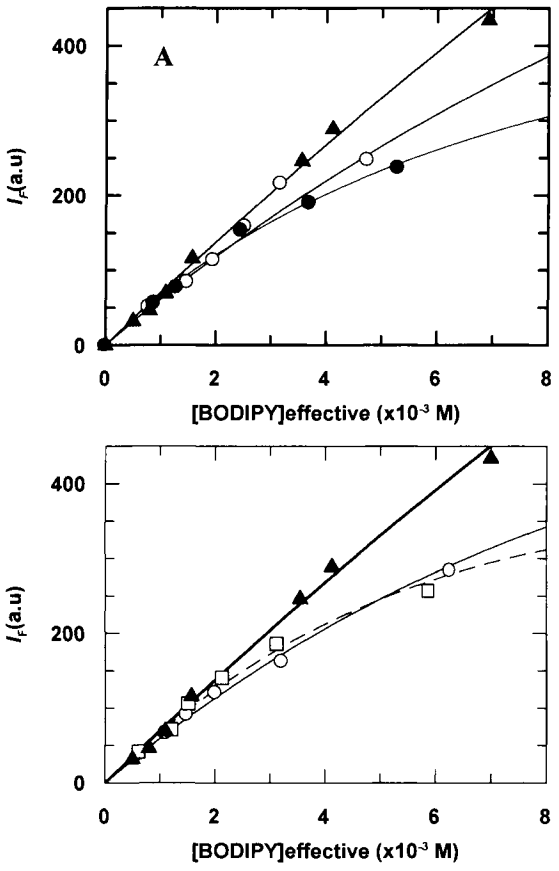

Figure 12.10. Fluorescence steady-state BODIPY self-quenching profile. A - Protein incorporated in DOPC (▲), DMoPC/DOPC (60/40 mol/mol) (○), and DEuPC/DOPC (60/40 mol/mol) (●). Eq.(20) is fitted to the data on the basis of dynamical quenching and a sphere-of-action quenching model (14.4 Å radius) (—) for the protein in all lipid systems. B – Protein incorporated in DOPC (▲), DMoPC (○), and DEuPC (□). Eq. (20) fit to data from DOPC bilayers using a sphere-of-action radius of 14 Å (—), from DEuPC bilayers with a sphere-of-action radius of 27 Å (---), and from DMoPC bilayers using a sphere-of-action radius of 23 Å (—). These higher values are evidence of aggregation. Reprinted from Fernandes *et al.* (2003) with permission. Copyright 2003 Biophysical Society.

The bimolecular quenching constants calculated from the self-quenching results for BD-M13 coat protein incorporated in DOPC, DMoPC/DOPC (60/40 mol/mol) DEuPC/DOPC (60/40 mol/mol), DEuPC, and DMoPC allow the estimation of the labeled protein molecular diffusion coefficient (D) using the Smoluchowski equation (Lakowicz, 1999), taking into account transient effects (Umberger and Lamer, 1945). For this

calculation and the validity of the 3D approach see sub-section 12.6.3. Taking 6 Å for BODIPY collisional radius, a value of 7.0×10^{-8} cm^2s^{-1} is obtained for $D_{\text{BD-M13 coat protein}}$ in DOPC bilayers, which has the same order of magnitude as the values of D for the M13 coat protein incorporated in fluid bilayers reported in the literature (Smith *et al.*, 1979, 1980).

However, for the lipid mixtures in which the predominant lipid does not hydrophobically match with the hydrophobic core of the M13 coat protein, the values obtained for D are unreasonably high. For the DMoPC/DOPC bilayers, a value of 4.2×10^{-7} cm^2s^{-1} is obtained, whereas in DEuPC/DOPC it is even higher (2.2×10^{-6} cm^2s^{-1}). If $D_{\text{BD-M13 coat protein}}$ in pure vesicles of DOPC is reporting a random distribution in the bilayer, the values in these mixtures are likely to be reporting protein segregation effects in the bilayer. This is caused by the hydrophobic mismatch constraints that the protein finds when incorporated in bilayers with too-long, or too-short phospholipids in their composition, leading to formation of localized areas with increased DOPC plus protein content. In this way, the apparent effective concentration in Eq. (19), should be higher than the one assumed on the basis of a random distribution, which led to an overestimation of $<k_q>$, and consequently of D.

This rationalization is supported by D values obtained from BODIPY labeled protein in the pure mismatching lipid DMoPC and DEuPC (Table 12.4). These values are smaller than the ones obtained from the mixtures, and the diffusion coefficient in pure DMoPC is almost identical to the value in pure DOPC. For pure vesicles of DEuPC, $D_{\text{BD-M13 coat protein}}$ is larger than in DOPC, but it is still much smaller than the value obtained from the DEuPC/DOPC mixture. These dynamic self-quenching results indicate therefore that, although in pure vesicles of DEuPC there are already more collisions between BODIPY groups than would be expected from a random distribution of labeled protein in the bilayer (probably due to aggregation), when DOPC is added the probability of collision increases greatly. At least in part, this can be explained in terms of protein segregation into DOPC-enriched microdomains. In DMoPC/DOPC the effect is similar, but the bimolecular quenching constant is smaller than in DEuPC/DOPC. In Figure 12.10, the obtained steady-state quenching profiles are presented together with the theoretical expectation for a sphere-of-action quenching model (Eq. 20). For the BODIPY-labeled protein in the DOPC-containing lipid systems (DOPC, DMoPC/DOPC, and DEuPC/DOPC) the results are well described using a sphere-of-action radius of 14 Å. For the pure mismatching lipids it is necessary to use larger radii to describe the results using Eq. (21).

In case that a complex is formed, the model to describe static quenching effects should take into account its equilibrium constant. For monomer/dimer equilibrium of only one molecular species, the fluorescence intensity is given by:

$$I_F = \frac{C\times[F]}{1/\tau_0 + < k_q > [F]} \times \frac{-1+\sqrt{1+8K_a[F]}}{4K_a} \tag{21}$$

where K_a is the oligomerization constant. However, for our system, in which there are two different protein species (labeled and unlabeled, where the unlabeled class includes both non-labeled mutant and wild-type protein), there will be several combinations of protein species within an aggregate. For a dimer, there will be three different combinations available—labeled protein/labeled protein, labeled protein/unlabeled

protein, and unlabeled protein/unlabeled protein—but only formation of the first one induces self-quenching of BODIPY. A complexation model describing fluorescence static quenching in our system will have to account for this fact. From the knowledge of the concentration of each species, the fraction of labeled protein participating in oligomers (dimers/trimers) containing more than one BODIPY labeled protein (and as a result non-fluorescent), can be obtained for a given K_a. The resulting set of nonlinear equations is promptly solved (for a given total protein concentration, labeling efficiency, labeled protein concentration, aggregation number, and K_a) using adequate mathematical software.

In Figure 12.11, a simulation was included for a small degree of protein aggregation in DOPC, DMoPC, and DEuPC bilayers. In these simulations it was considered that, due to the small degree of self-association considered, there was no change in M13 coat protein distribution and dynamics, and that in an oligomer, the fluorescence intensity of a BODIPY group is reduced to zero by the presence of another BODIPY group in the same aggregate. For DOPC bilayers, the prediction using a low fraction of aggregation (25% for dimerization and 10% for trimerization) clearly overestimates the extent of aggregation at the high labeled protein concentration, the range where this methodology is more sensitive. In agreement, from Figure 12.10, it is clear that the data for the three DOPC-containing lipid systems are rationalized on the basis of dynamic quenching and a sphere of action, without need for assumption of aggregation. The recovered radius (R_S = 14 Å) is close to the sum of the Van der Waals radii. These results indicate that BD-M13 coat protein in the studied DOPC-containing bilayers does not oligomerize. This conclusion is further supported by the absence of BODIPY dimers in our samples, which would be revealed in the absorption/emission spectra.

Still, the results from self-quenching on pure bilayers of hydrophobic mismatching lipids (DEuPC and DMoPC) point to some aggregation, as the sphere-of-action radii recovered from the fit of Eq. (20) were very unrealistic (27 Å and 23 Å for DEuPC and DMoPC, respectively). Simulations for BODIPY emission self-quenching due to aggregation are compared with the experimental data in these lipid systems in Figure 12.11. DMoPC data could be reasonably described using a K_a = 20 for dimerization and a K_a = 1300 for trimerization (13% of aggregated protein at the protein concentration of the most concentrated data point in both simulations).

For the data obtained in DEuPC, the degree of aggregation is higher than in DMoPC (a larger sphere-of-action radius was recovered from the fit of Eq. (20)). This result is in agreement with the observations of Meijer *et al.* (2001), who, from ESR studies, reported that the protein appeared to exist in several orientations/conformations or in an aggregated form while incorporated in DEuPC bilayers. The larger extent of coat protein aggregation observed in the longer lipid bilayers can be explained by the fact that negative hydrophobic mismatch is considered to be energetically less favorable than positive mismatch (Killian, 1998; Mall *et al.*, 2001).

Regarding the DEuPC/DOPC and DMoPC/DOPC lipid mixtures used in the present study, no change in conformation or orientation was found (CD spectroscopy/IAEDANS fluorescence emission spectra, not shown), and, as described above even for the protein in DEuPC/DOPC (60/40 mol/mol) no aggregation was detected (BODIPY self-quenching). These results point to stabilization of the protein by the hydrophobic matching phospholipid (DOPC), which was probably achieved by protein segregation to

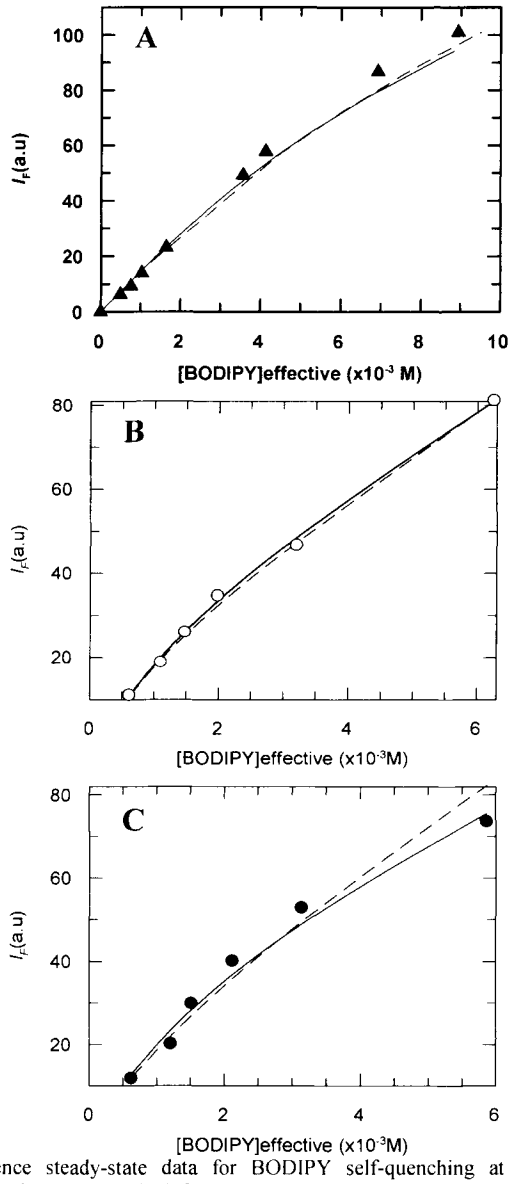

Figure 12.11. Fluorescence steady-state data for BODIPY self-quenching at different labeled protein concentrations. A- Protein incorporated in DOPC (▲) and simulations considering protein oligomerization including static quenching: (—) due to trimerization of the protein with K_a = 1000 (≈ 10% total protein oligomerization). (---) due to dimerization of the protein with K_a = 10 (≈ 25% total protein oligomerization). B- Protein incorporated in DMoPC (○) and simulations for dimerization of protein with K_a = 20 (≈ 13% total major coat protein oligomerization for the most concentrated data point) (---), and trimerization of the protein with K_a = 1300 (≈ 13% total M13 coat protein oligomerization for the most concentrated data point) (—). C - Protein incorporated in DEuPC (●) and simulations for dimerization of protein with K_a = 30 (≈ 17% total protein oligomerization for the most concentrated data point) (---) and trimerization of the protein with K_a = 7500 (≈ 25% total protein oligomerization for the most concentrated data point) (—). Reprinted from Fernandes *et al.* (2003) with permission. Copyright 2003 Biophysical Society.

domains enriched in that phospholipid, partly explaining the high M13 coat protein apparent molecular diffusion coefficients obtained for the protein incorporated in DEuPC/DOPC and DMoPC/DOPC bilayers.

Although an increase in BODIPY emission dynamic self-quenching was already visible for pure DEuPC bilayers, the bimolecular diffusion rate constant value in DEuPC/DOPC bilayers is much higher, and still, this can only be explained by segregation to DOPC-enriched microdomains.

12.6.2. Headgroup and Acyl Chain-Length Effects on Lateral Distribution of M13 Major Coat Protein Studied by FRET

The energy transfer study was performed using IAEDANS –labeled protein as donor and BODIPY-labeled as acceptor, due to the good overlap of the former's emission with the latter's absorption. Energy transfer studies were performed for the labeled protein incorporated in DOPC, DOPC/DOPG (80/20 mol/mol), DOPE/DOPG (70/30 mol/mol), DEuPC/DOPC (60/40 mol/mol), and DMoPC/DOPC (60/40 mol/mol). It was intended to study the influence of electrostatic interactions and hydrophobic mismatch in the aggregation and compartmentalization properties of the M13 coat protein. Due to the nonlamellar character of phosphatidylethanolamines (PE), it was necessary to include a fraction of lamellar lipids (phosphatidylglycerol, PG) in the lipid mixture for bilayer stabilization.

Experimental energy transfer efficiency is obtained from

$$E = 1 - I_{DA}/I_D \tag{22}$$

where I_D and I_{DA} are the donor fluorescence intensities in absence and presence of acceptor, respectively. To obtain topological information, this observable should be compared with theoretical expectations.

For the in-plane FRET, the decay of donor fluorescence in the presence of acceptor, assuming a radius of exclusion of acceptors (R_e) around the donor (in this case the sum of the van der Waals radii of the chromophores), and a random distribution in the plane of the membrane considered as infinite, becomes (Wolber and Hudson, 1979):

$$\rho_{ex}(t) = \exp\left\{-\pi R_0^2 n_2 \gamma\left[\frac{2}{3},\left(\frac{R_0}{R_e}\right)^6\left(\frac{t}{<\tau>}\right)\right]\left(\frac{t}{<\tau>}\right)^{1/3} + \pi R_e^2 n_2\left(1-\exp\left[-\left(\frac{R_0}{R_e}\right)^6\left(\frac{t}{<\tau>}\right)\right]\right)\right\} \tag{23}$$

where R_0 is the Förster radius (see below), n_2 is the acceptor numerical density (number of acceptors per unit area), and

$$\gamma(x,y) = \int_0^y z^{x-1}\exp(-z)dz \tag{24}$$

is the incomplete Gamma function.

From these equations and admitting that $R_0 >> R_e$ (as verified in our study) Wolber and Hudson (1979) obtained the analytical solution for energy transfer efficiencies:

$$E = 1 - \sum_{j=0}^{\infty} \left(-\pi\Gamma(2/3)R_0^2 n_2\right) \times \frac{\Gamma(j/3+1)}{j!} \tag{25}$$

where Γ is the complete gamma function (which is given by Eq. (24) when the upper limit of the integral is ∞).

The Förster radius is given by:

$$R_0 = 0.02108 \cdot \left[\frac{\left(\int \lambda^4 \varepsilon(\lambda) f(\lambda) d\lambda\right) \kappa^2 \Phi_D}{n^4} \right]^{1/6} \tag{26}$$

where κ^2 is the orientation factor, n is the refractive index of the medium, Φ_D is the donor quantum yield, $f(\lambda)$ is the normalized emission spectra of the donor and $\varepsilon(\lambda)$ is the absorption spectra of the acceptor. If the λ units in Eq. (26) are nm, the calculated R_0 has Å-units (Berberan-Santos and Prieto, 1987).

For our pair, using $\Phi_D = 0.64$ (determined in this study) and assuming $\kappa^2 = 2/3$ (the isotropic dynamic limit) and $n = 1.4$ (Davenport *et al.*, 1985), we obtain $R_0 = 49$ Å. The value $\kappa^2 = 2/3$ was considered because for fluorophores in the centre of a fluid bilayer, the rotational freedom should be sufficiently high to randomize orientations. This is supported by the reasonably low steady-state anisotropy values obtained for the IAEDANS and BODIPY probes labeled on the T36C M13 coat protein mutant ($\langle r \rangle_{AEDANS} = 0.14$, $\langle r \rangle_{BODIPY} = 0.23$; for a detailed discussion, see Loura *et al.*, 1996).

The results for BD-M13 coat protein in DOPC, DOPC/DOPG, DOPE/DOPG, DMoPC/DOPC, and DEuPC/DOPC bilayers are presented in Figure 12.12. The centered position of BODIPY in the bilayer allows for a simplification of the energy transfer analysis for a two-dimensional situation, as described by Eq. (25), *i.e.*, there is no need to consider interplanar (bilayer) FRET geometry (Loura *et al.*, 2001a; this situation is described in Section 12.7). Simulations of energy transfer for random distribution of acceptors using Eq. (25) can therefore be compared with our experimental results (Figure 12.12). The energy transfer efficiencies obtained for BD-M13 coat protein in the DMoPC/DOPC and DEuPC/DOPC bilayers support the other results discussed above for these mixtures, as they can only be explained by protein segregation in the bilayer or severe aggregation (Figure 12.12 B). However, as discussed above, the data obtained by fluorescence emission self-quenching indicate that segregation into DOPC-enriched domains (rather than aggregation) is the major phenomenon in these lipid mixtures.

Although the results can be reasonably explained on the basis of protein segregation to 60% of the total bilayer area (Figure 12.12 B), this rationalization should be considered an oversimplification, and is presented as an illustration. Indeed, the measured efficiencies are only reporting the average BD-M13 coat protein surface density that each IAEDANS-labeled protein is sensing. Probably there will be M13 coat protein interacting with the mismatching phospholipids, but the majority of the proteins will be preferentially surrounded by DOPC, and microdomains enriched in DOPC and M13 coat protein should be formed.

The lipid mixtures used in this work for hydrophobic matching studies (DMoPC/DOPC and DEuPC/DOPC) are thought to be considerably closer to ideality

than the ones used in the studies of gel/fluid coexistence by Dumas *et al.* (1997), and of natural and pyrene-derivatized lipids by Lehtonen and Kinunnen (1997). However, protein segregation was observed in our study for both DMoPC/DOPC and DEuPC/DOPC, whereas in DOPC random distribution of protein in the bilayer was confirmed. Also interestingly, the degree of segregation appears to be similar for both mixtures (Figure 12.12 B), which was not expected due to the observed larger aggregation degree of coat protein in DEuPC, and therefore to an apparent larger packing difficulty with the longer lipid.

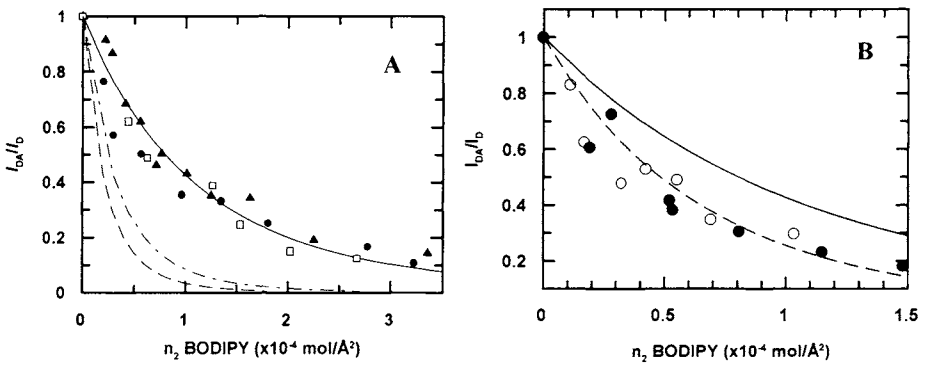

Figure 12.12. A - Donor (IAEDANS) fluorescence quenching by energy transfer acceptor (BODIPY). (▲) - Experimental data for DOPC, (●) – DOPC/DOPG (80/20 mol/mol) and (□) – DOPE/DOPG bilayers. (70/30 mol/mol). (—) - Theoretical expectation (Eq. 25) for a random distribution of acceptors. Energy transfer simulation for total co-localization of M13 coat protein considering 20% (----) and 30% (— - —) of the total surface area available. B - Donor (IAEDANS) fluorescence quenching by energy transfer acceptor (BODIPY). (—) - Theoretical expectation for a random distribution of acceptors. (---) - Simulation for a segregation of major coat protein considering 60% of the total surface area available. (●) - Experimental data for DEuPC/DOPC (60/40 mol/mol), (○) –experimental data for DMoPC/DOPC (60/40 mol/mol). I_{DA} and I_D were obtained by integration of donor decays. Reprinted with pemission from Fernandes *et al.* (2003). Copyright 2003 Biophysical Society.

The formation of local structures within the thermodynamic fluid phase (see Introduction Section) for a mixture of two PCs with a 4-carbon difference in acyl-chain lengths (DMPC/DSPC) was theoretically predicted by Mouritsen and Jørgensen (1994). The clusters size in the Monte-Carlo configurations obtained by these authors appears to be very small (10–20 molecules at most). However, significant alterations in FRET efficiency, as measured by Lehtonen *et al.* (1996) in mixtures of unsaturated PCs, and by us between IAEDANS-labeled protein and BODIPY-labeled protein, require that the domain size should be of the order of magnitude of R_0, which is $\cong$ 5 nm. In our system, this large domain size might be a consequence of protein-induced phase separation.

In this work we also studied whether similar heterogeneities could be induced by the presence of positively charged M13 coat protein in bilayers composed of mixtures of anionic and neutral phospholipids. Due to the basic character of M13 coat protein C-terminal, it is reasonable to consider the possibility of anionic phospholipid-enriched domain induction by M13 coat protein incorporation in the bilayer. The formation of these domains could actually help explain some of the mechanisms involved in the creation of the phage assembly site.

Assuming that the hypothetical domains were composed by all the protein and DOPG content in the sample, and that the protein would be randomly distributed inside them, we can, using Eq. (25), obtain theoretical curves describing the energy transfer within these domains. These plots are compared with the experimental data points for M13 coat protein incorporated in DOPC/DOPG (80/20 mol/mol) and DOPE/DOPG (70:30 mol/mol) in Figure 12.12 A. It is concluded that the segregation of M13 coat protein to a PG-rich phase in the mixed systems, induced by electrostatic interactions between the positively charged protein and the negatively charged phospholipid, is ruled out. In fact, this process would lead to a greater local surface density of acceptor, and therefore, a very significant increase of energy transfer efficiencies should be observed, contrary to the data.

On the whole, from this study, it is clearly concluded that the M13 coat protein monomeric state is highly stable when incorporated in bilayers containing hydrophobic matching phospholipids, which had been suggested in other studies (Stopar *et al.*, 1997; Spruijt *et al.*, 1989; Sanders *et al.*, 1991). The lack of anionic phospholipids has no effect on the protein oligomerization properties at the protein concentrations used in this study. When the protein is incorporated in pure vesicles of mismatching lipid there is evidence for protein aggregation but for mixtures of lipids containing both hydrophobic-matching (DOPC) and -mismatching (DEuPC or DMoPC) phospholipids, the protein probably segregates to domains enriched in DOPC, which can explain the stability of the monomeric species of the protein in these lipid systems. This segregation effect is only observed when hydrophobic mismatching phospholipids are present, suggesting that the hydrophobic matching conditions on the protein-lipid interface are more important than electrostatic interactions between the M13 coat protein and the phospholipids, for the protein lateral distribution on the bilayer.

12.6.3. γM4 Lateral Distribution from Fluorescence Self-Quenching Studies

In the case of the peptide γM4 from the muscle AChR, the presence of a dynamic self-quenching process gave valuable information on the lateral distribution of peptide in the chol-poor ld phase *vs.* the chol-rich lo phase (de Almeida *et al.*, 2004).

The fluorescence of the γM4 peptide incorporated in multilamellar vesicles (MLV) made of POPC/chol (60:40 mol/mol) is shown in Figure 12.13. The spectral position (not shown) and the steady-state anisotropy, $\langle r \rangle$ (Table 12.5), are insensitive to the presence of chol, *i.e.*, they are the same in ld or lo phases, and the anisotropies are reasonably high and typical of a Trp-containing peptide strongly immobilized in a membrane.

The lifetime-weighted quantum yields $\langle \tau \rangle$, both for the ld and lo phases, are shown in Table 12.5 for several γM4 peptide concentrations. In the ld phase, upon increasing the concentration from 0.7 mol% up to 7 mol%, the Trp lifetime-weighted quantum yield was reduced to one-half. This can be accounted for by the presence of Cys and Lys residues in the γM4 transmembrane domain, which are known to be efficient quenchers of Trp fluorescence (Chen and Barkley, 1998). Thus, at higher concentrations the proximity between γM4 peptides leads to a decrease of the Trp intrinsic fluorescence due to an intermolecular self-quenching process.

Table 12.5. Photophysical properties of the Trp^{453} residue in the γM4 peptide incorporated into POPC/chol vesicles with low (ld phase) or high (lo phase) chol content at room temperature. λ_{exc} = 288 nm and λ_{em} = 340 nm. The concentration of γM4 peptide is expressed in mol% relative to total lipid. See text for further details.

γM4 (mol %)	$\langle\tau\rangle_{ld}$ (ns)	$\langle\tau\rangle_{lo}$ (ns)	$\bar{\tau}_{ld}$ (ns)	$\bar{\tau}_{lo}$ (ns)	$\langle r\rangle_{ld}$	$\langle r\rangle_{lo}$
0.7	3.04±0.05	1.47±0.10	4.29	2.84	0.089±0.006	0.091±0.012
3.0	2.11±0.08	1.44±0.11	3.53	2.69	0.078±0.007	0.076±0.006
7.0	1.43±0.08	—	2.81	-	0.080±0.008	-

Reprinted with permission from de Almeida *et al.* (2004). Copyright 2004 Biophysical Society.

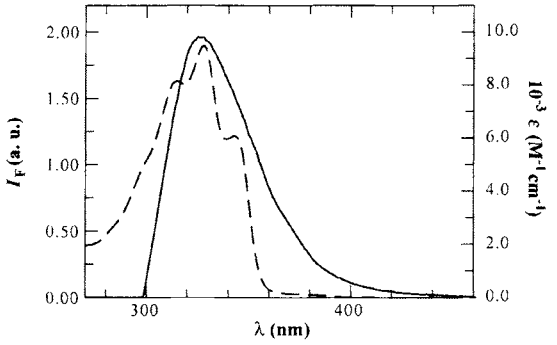

Figure 12.13. Emission spectrum of γM4 (λ_{exc} = 288 nm) in POPC vesicles (solid line) and absorption spectrum of DHE in POPC/chol (3:2) vesicles (dotted line) at room temperature. Reprinted with permission from de Almeida *et al.* (2004). Copyright 2004 Biophysical Society.

For the lo phase, the lifetimes do not show such a strong variation, and in addition, the values for the lower concentrations (0.7% and 3 %) in lo are close to those found for the higher concentrations in ld (7 %). Also, as the dynamic self-quenching mechanism depends on the quencher concentration sensed by the fluorophore, in the case of γM4 in chol-rich vesicles, a higher effective peptide concentration occurs, augmenting the extent of the self-quenching process (the quenching process in this case is that of Trp fluorescence by other residues of the peptide, and thus is not exactly the same as described for M13, where only the fluorophore group is involved in the quenching process).

The effect of the collisional contribution of self-quenching on the fluorescence lifetime for a molecule with a complex decay is described by the Stern-Volmer equation (Eq. 19). In this case, the calculation is performed separately for each concentration, and thus $\bar{\tau}_0$ can be replaced by $\bar{\tau}_{0q}$, which is given by (Sillen and Engelborghs, 1998):

$$\bar{\tau}_{0q} = \sum_i a_{0i}\tau_i\tau_{0i} \Big/ \sum_i a_{0i}\tau_i \tag{27}$$

The subscript 0 indicates again the absence of quencher.

The bimolecular quenching rate constant $<k_q>$ is related to the diffusion coefficient of the fluorophore (D) via the Smoluchowski equation (Lakowicz, 1999), taking into account transient effects (Umberger and Lamer, 1945):

$$< k_q >= 4\pi N_A (2R_c)(2D)\left[1 + 2R_c/(2\bar{\tau}_{0q} D)^{1/2}\right] \quad (28)$$

where N_A is the Avogadro constant and R_c is the collisional radius.

This equation assumes diffusion in an isotropic 3D medium. If the membrane were strictly bidimensional, different boundary conditions for the Smoluchowski formalism could be applied (Razi-Naqvi, 1974). The best approach to the specific situation of probe diffusion in a membrane is the one used by Owen (1975), in which the finite bilayer width (cylindrical geometry) is taken into account. Owen introduced the parameter τ_s, which defines the transition from the spherical (3D) to the cylindrical geometry, its value being τ_s = 16 ns when considering the bilayer (Wiener and White, 1992) and the peptide/Trp (Zamyatnin, 1972) parameterization. This value of τ_s is much longer than the longest fluorescence lifetime of Trp^{453} in the γM4 peptide (~ 5 ns), and longer than our experimental time-window (15.3 ns = 15.3 ps/channel ×1,000 channels); the 3D framework approximation is therefore essentially correct. If we consider that the lifetime-weighted quantum yield of the more diluted γM4 peptide concentration is the limiting $<\tau>_0$ (no quenching occurring) (Table 12.5), a value of $<k_q> = 2.6\times10^9$ mol^{-1} dm^3 s^{-1} is obtained from Eq. (19) for the 7 mol % peptide concentration. This value assumes a random peptide analytical concentration in the lipid $[F] = 0.083$ M^{-1}, determined on the basis of its 7 mol % concentration and considering a volume for the POPC molecule of 1,263 $Å^3$ (Small, 1986). A similar value ($<k_q> = 2.8\times10^9$ mol^{-1} dm^3 s^{-1}) could be obtained for the other peptide concentration, 3%.

If in Eq. (28) we assume the collisional radius for the dimer to be 10 Å, diffusion coefficients of D = 14 $\times10^{-8}$ cm^2 s^{-1} (for 7% peptide) and D = 12 $\times10^{-8}$ cm^2 s^{-1} (for 3% peptide) are obtained. These values have the same order of magnitude or are slightly higher than those typically found for diffusion in an ld phase (D = 1.1$\times10^{-8}$ cm^2 s^{-1} (Dietrich *et al.*, 2001), D = 1-3 $\times10^{-8}$ cm^2 s^{-1} for transmembrane proteins and D = 9-14 $\times10^{-8}$ cm^2 s^{-1} for a fluorescent lipid derivative (Vaz *et al.*, 1982). Although this is a comparison with values obtained from fluorescence recovery after photobleaching studies of large proteins or from phospholipid single particle tracking studies, the agreement is reasonably good within the framework of the approximations used.

It is interesting to note that in pure lo phase, for the lower peptide concentration studied, the lifetime is already quite low (Table 12.5) and similar to the value for the highest concentration in ld phase. As previously described, self-quenching was observed for a single ld phase (it is known that several amino acid side-chains are effective quenchers of Trp fluorescence), and therefore only a higher effective peptide concentration can be invoked to rationalize the lo data. This means that the peptide is not randomly distributed in the lo phase and that patches with a higher local concentration of γM4 are formed. Within the framework of a Stern-Volmer analysis (Eq. 19), this higher peptide concentration gives rise to a higher decrease in lifetime. It can therefore be concluded that the formation of γM4 peptide-rich patches is strongly induced by chol.

12.6.4. FRET from γM4 (Trp^{453}) to Dehydroergosterol (DHE): Sterol Segregation in a One-Phase System *vs.* Peptide-Rich Patches

In order to obtain information on the affinity of the γM4 peptide for chol, FRET measurements were carried out using Trp^{453} and the fluorescent chol analogue DHE as donor and acceptor, respectively. In this series of experiments the totally reduced monomeric species of γM4 was used, since the disulfide-bonded dimer would introduce an additional complexity in the analysis of FRET data: two Trp donors would be present in the dimer, the system topology would lose cylindrical symmetry around each donor, and a complex geometry regarding the excluded volume for transfer would have to be considered. To further reduce the complexity of the system, the monomeric γM4 species was reconstituted in small unilamellar vesicles (SUV) in order to avoid a multilayer geometry and to minimize light scattering data biasing. Another important advantage of SUV relative to larger model membranes is the absence of DHE tail-to-tail dimerization that is observed in 100 nm diameter vesicles (Loura and Prieto, 1997) and which would also render the analysis of the FRET results more difficult. DHE has no bulky fluorophores in its structure, thus lacking the disadvantages of other chol analogs, which were shown to be excluded from chol-rich phases (Loura *et al.*, 2001b). At the chol concentration at which the FRET study was carried out (40 mol %), the system is largely in the lo phase (Mateo *et al.*, 1995; de Almeida *et al.*, 2003; Figure 12.2). The complexity of studying FRET in a biphasic system (Loura *et al.*, 2001a) is therefore circumvented. The typical radius for a SUV (~25-50 nm) is much larger than 1.5 R_0, and the system can be safely assumed as being planar with respect to FRET (Eisinger *et al.*, 1981).

The Förster radius was calculated next from the experimental data in Figure 12.13 -the donor's emission (Trp^{453}) and the acceptor's (DHE) absorption. Values of $\kappa^2 = 2/3$, and $n = 1.44$ (Davenport *et al.*, 1985) were considered in Eq. (26). The fluorescence quantum yield $\Phi_D = 0.067$ was estimated on the basis of the Trp lifetime-weighted quantum yield as compared to that of *N*-acetyltryptophanamide, a well-known model for this amino acid residue within a polypeptide chain (Szabo and Rayner, 1980). This procedure avoids all the errors related to the determination of quantum yields in scattering media using steady-state data, and it does not take into account effects of static quenching by sulphydryl groups. A value of $R_0 = 20$ Å was obtained.

The fluorescence decay of Trp^{453} is described by a sum of three exponentials, and for the determination of FRET efficiency, *E*, decay integration was carried out in order to determine the lifetime-weighted quantum yield:

$$E = 1 - \left(\int_0^\infty i_{DA}(t)dt \right) / \int_0^\infty i_D(t)dt = 1 - <\tau>_{DA} / <\tau>_D \tag{29}$$

where $i_D(t)$ and $i_{DA}(t)$ are the fluorescence decays of donor in the absence and presence of acceptor, respectively. It should be pointed out that this study could not be carried out using steady-state techniques (Eq. 22) due to the strong absorption overlap of donor and acceptor, leading to large inner filter effects, and the low steady-state intensities for the reduced species, preventing the measurement of reliable absolute intensities. The variation of *E* upon increasing acceptor concentration is shown in Figure 12.14. FRET efficiency was found to be lower than that expected on the basis of a random distribution.

The theoretical expectation for a random distribution of acceptors (Figure 12.14) involves consideration of the following structural features: i) The peptide helix was approximated to a cylinder with 10 Å diameter (Bowie, 1997), with the donor located at the axis; ii) the peptide was allowed to incorporate into the bilayer in either direction, *i.e.*, the Trp^{453} donor can be located close to any of the two membrane/water interfaces, and DHE can in turn be located on either leaflet. Because R_0 is not small with respect to the membrane thickness, both in-plane (Eq. 23) and out-of-plane (Eq. (36) in the next section) transfer to acceptors in the other membrane leaflet were considered (the interplanar donor-acceptor distance was fixed as w = 22 Å on the basis of molecular models). In the calculation of the surface density of acceptors, the condensing effect of chol on the lipid surface was taken into account (~7Å^2 / molecule; Smaby *et al.*, 1997), together with an area/molecule of 66.4 Å^2 for POPC (Chiu *et al.*, 1999) and 37.7 Å^2 for chol (Smaby *et al.*, 1997).

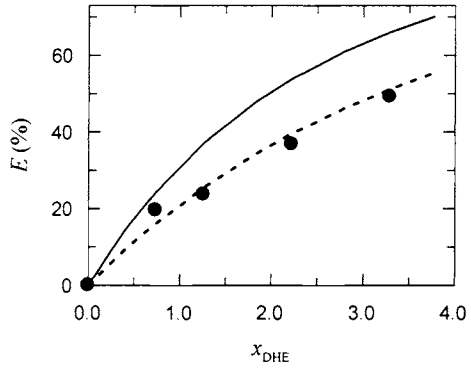

Figure 12.14. FRET efficiency from γM4 (reduced monomeric species) Trp^{453} to DHE (R_0 = 20 Å) *vs.* acceptor mole fraction. The circles are experimental data points. The solid line is the calculated FRET efficiency for a random distribution of acceptors in the plane of the membrane with an exclusion radius of 5 Å, to account for the area occupied by the donor containing α-helix. Both in-plane and out-of-plane (interplanar distance of 22 Å) FRET are considered. See text for further details on the calculations. The dotted line is also based on a random distribution model considering only 62% DHE molecules available as acceptors. Reprinted with permission from de Almeida *et al.* (2004). Copyright 2004 Biophysical Society.

The experimentally determined values of FRET efficiency, E, were significantly lower than expected, and the data could only be rationalized with an effective sterol concentration ~ 38% lower than the analytical expected concentration (see Figure 12.14). This does not necessarily mean that there is a tendency to exclude the sterol away from the γM4 peptide vicinity, but the area available for the dispersion of sterol is probably reduced because of the formation of peptide rich-patches. This estimated area reduction can, in turn, be compared with that derived from the above-mentioned self-quenching data. The same degree of quenching is obtained for 7 mol% peptide in ld and for all concentrations in lo. Since the diffusion coefficient in lo is 3-fold lower than in ld (*e.g.* Dietrich *et al.*, 2001), it can be assumed that the effective concentration of peptide is 3-fold higher in the patches. Using the area per lipid molecule for the lo phase (computed

as described above) it can be concluded that the γM4 peptide occupies ~30% of the area in the patches in agreement with the FRET data.

12.6.5. γM4 Structure and Organization from Energy Homotransfer Studies

In the absence of a reducing agent, and because there is a Cys residue in the peptide sequence, γM4 has the ability to form dimers, although the monomeric species predominates (as concluded from polyacrylamide gel electrophoresis in denaturing conditions). The dimer has two Trp^{453} residues, one in each helix, which can lead to energy homotransfer (energy migration) between these two Trp residues. This interaction can be used to obtain structural information (distances) on the peptide (de Almeida *et al.*, 2004). As a consequence of energy migration, Trp anisotropy may decrease. The expected value for the dimer anisotropy $\langle r \rangle_D$ can be determined following, *e.g.*, Runnels and Scarlata (1995), as

$$\langle r \rangle_D = \langle r \rangle_M (1+(R_0/l)^6)/ (1+2(R_0/l)^6) + \langle r \rangle_{ET} (R_0/l)^6/(1+2(R_0/l)^6 \quad (30)$$

where l is the distance between the two chromophores, R_0 is the Förster radius for energy migration, $\langle r \rangle_M$ is the anisotropy of the initially excited molecule, and $\langle r \rangle_{ET}$ is the anisotropy of the second molecule of the pair. This second contribution can be disregarded because it is smaller than 4% of the first one at all times (Berberan-Santos and Valeur, 1991). To obtain the inter-Trp distance, we fed the experimentally determined value of $\langle r \rangle_D$ for the dimer into Eq. (30). In the energy heterotransfer experiments described in the previous sub-section, the reduced species, *i.e.*, the monomer was used. However, the monomer anisotropy $\langle r \rangle_M$ could not be evaluated because of the strong fluorescence quenching produced by the -SH group in Cys^{451}. This fact also rules out any biasing of steady-state anisotropy data, due to the presence of the monomeric species. The steady-state intensity was too low to yield reliable data. We therefore resorted to literature values from a systematic study of time-resolved anisotropy in which Trp were introduced in different positions along an α-helical peptide in a fluid membrane (Vogel *et al.*, 1988). Trp residues located near the surface, such as Trp-1, or at a shallow position in the hydrocarbon core, such as Trp-6 in the cited work (a condition identical to that of the γM4 peptide under study), constitute a suitable model to obtain $\langle r \rangle_M$.

We calculated the steady-state anisotropy by integration of the reported time-resolved data of Vogel *et al.* (1988) according to $i(t) = \Sigma_i a_i \exp(-t/\tau_i)$ and Eq. (11). The steady-state anisotropy results from:

$$\langle r \rangle = \int_0^\infty i(t)r(t)dt \Big/ \int_0^\infty i(t)dt \quad (31)$$

In this equation, both the lifetime data of Vogel *et al.* (1988) and our own were used, leading in both cases to an identical value for the anisotropy: $\langle r \rangle_M = 0.082 \pm 0.013$, which is not significantly different from that obtained for the dimeric peptide in the present study (Table 12.5). It can therefore be concluded that there is no relevant energy migration in the dimer, allowing us to set a lower boundary for the inter-Trp distance.

A Förster radius $R_0 = 10$ Å for energy migration was calculated according to Eq. (26) considering $\Phi_D = 0.13$. This value was obtained again by comparing the lifetime-

weighted quantum yields of the γM4 peptide and that of *n*-acetyltryptophanamide. From Eq. (30) it is predicted that for interchromophore distances larger than $\approx 2R_0$, the degree of depolarization as a consequence of energy migration is insignificant. This corresponds to a distance of 20 Å in the present case. In fact, for two helices connected by a disulfide bond, each Trp residue would be in an approximately diametrically opposed position, because for an ideal α-helix, an arc of ~200° would be subtended between Trp^{453} and Cys^{451} (Figure 12.15 A).

Now that intra-peptide energy migration was discarded, the reasons why anisotropy is largely concentration-independent (Table 12.5), *i.e.*, the lack of efficient intermolecular energy migration in either the ld or lo phases, should be discussed.

Before this analysis, the decrease in fluorescence lifetime due to the intermolecular collisional self-quenching must be considered. It should be stressed that energy migration does not affect the lifetime or intensities, *i.e.*, there is no quenching (Valeur, 2001) and only anisotropy decreases. However, the decrease in lifetime by some other mechanism results in an increase in anisotropy (Eq. 13). Thus the decrease in anisotropy due to energy migration would be hidden due to a compensatory reduction in fluorescence lifetime, as described in Section 12.5. Considering Eq. (13), a value of limiting anisotropy $r_\infty = 0.066$ (experimentally determined), and $r_0 = 0.173$ for excitation at $\lambda = 288$ nm (Valeur and Weber, 1977), a global rotational correlation time $\varphi = 1$ ns is obtained.

These result facilitates the determination of the expected anisotropies for the higher concentrations (3% and 7%); they are $\langle r \rangle = 0.090$, and $\langle r \rangle = 0.094$, respectively. As can be seen, they are very close to the experimentally determined ones (Table 12.5), *i.e.*, the decrease in fluorescence lifetime does not imply a significant variation of anisotropy. This is certainly related to the large residual anisotropy.

From the invariance of anisotropy with concentration it can safely be concluded that there is no significant intermolecular energy migration. For the energy migration in a bi-dimensional system such as a membrane, Snyder and Freire (1982), from Monte-Carlo simulations, obtained a decrease in anisotropy for a random distribution of fluorophores in a membrane (and although this was derived for an isotropic rotor, it is relevant to compare these expectations with our data). Considering the Förster radius, $R_0 = 8.5$ Å, as described above (but now calculated from a lower quantum yield, reflected in an also lower lifetime-weighted quantum yield, Table 12.5), and using the data from Figure 12.9 in the work of Snyder and Freire (1982), it can be concluded that for the highest concentration of γM4 studied here (7%, which corresponds to 0.22 molecules within a circle of radius R_0), the reduction in anisotropy should be at most 15%, in full agreement with our data.

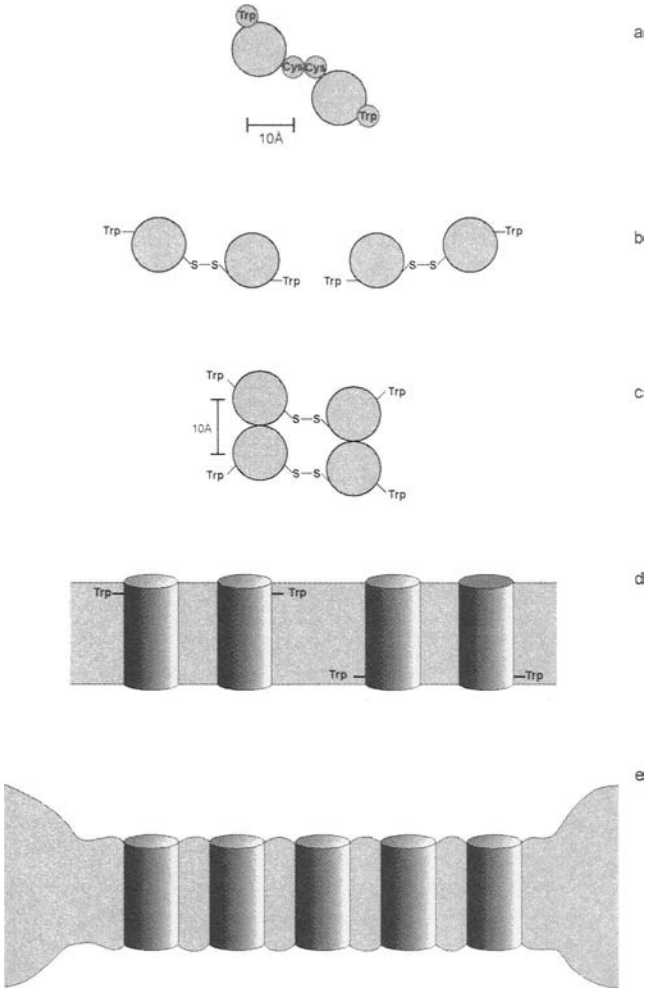

Figure 12.15. Putative organization of γM4 in chol-poor and chol-rich systems. A plausible structural framework to account for the absence of energy migration between Trp^{453} residues in the γM4 peptide, and the variation of lifetime-weighted quantum yield with peptide concentration on the ld and lo phases is provided. A) Top view of the α-helical peptide showing the relative positions of Trp^{453} and Cys^{451}, and a probable geometry for a disulfide bonded dimer. B) Possible geometry for a linear aggregate. This structure is ruled out. C) Parallel aggregate in end-on view. This structure is not ruled out by energy homotransfer data. D) Anti-parallel aggregate, lateral view. This structure is not ruled out by energy homotransfer data. E) Peptide-rich patch. The model depicts the distribution of γM4 in POPC/chol vesicles with high chol content (lo phase). The negative mismatch causes a disordering effect in the vicinity of a peptide molecule, and other peptides accommodate better in a region close to where other peptides localize. In the ld (chol-poor phase) the peptide is randomly distributed due to the very good matching between the hydrophobic thickness of the bilayer and the peptide. Reprinted with permission from de Almeida *et al.* (2004). Copyright 2004 Biophysical Society.

From the self-quenching experiments, it was concluded that peptide-rich patches occur, at least in the lo phase. Because no energy migration is operative, and due to the small Förster radius for migration, we can obtain structural information about these patches. The absence of energy migration implies that: i) there is no molecular contact of Trp residues in one dimer with those of another dimer. This indicates that no linear aggregates are formed (Figure 12.15 B). If this type of dimer-dimer contact did occur, a strong decrease in anisotropy such as, for example, observed for DHE (Loura and Prieto, 1997) would take place. ii) The formation of dimer "parallel" aggregates cannot be discarded (Figure 12.15 C). For this geometry, an inter-Trp minimum distance of 10 Å could be expected. The anisotropy would drop to 78% of its initial value (Eq. 30), and if a small enough fraction of these aggregates were formed, this would not entail high global migration efficiency. It should be stressed that as stated above for the intramolecular process, there would be no transfer for the other two Trp residues. Anyway, anti-parallel inter-helical contacts (Figure 12.15 D) would not produce significant depolarization because the Trp residues would be too far apart, *i.e.*, they would be separated by at least the hydrophobic thickness of the bilayer. The method employed in this work to obtain peptide-containing vesicles cannot discard the occurrence of both possible peptide orientations in the bilayer. It is known, in addition, that anti-parallel contacts are more probable due to stabilization by the opposite sign macrodipole moment in the anti-parallel helix (Bowie, 1997) and in lo, with a larger hydrophobic thickness, less of the helix termini should protrude to the solvent, thus decreasing solvent screening and increasing the strength of the dipole-dipole interaction relative to ld. This can allow for other types of helix-helix interactions like close packing (note that at the extreme of the hydrophobic helix opposite to the Trp^{453} side, there is a threonine (Thr^{469}) and a glycine residue (Gly^{470}), both with small side chains that should favor helix approximation, in addition to Gly^{462} and Thr^{463}, approximately in the middle of the γM4 helix).

If the γM4 peptide formed linear aggregates, there would be no significant interhelix stabilization. This effect is maximal for the case of anti-parallel dimers. However, there would be no need to invoke such a limiting situation if long-range interactions were operative. As shown in Figure 12.15 *E*, patches could be formed with no direct molecular contact, *i.e.*, a small number of lipid molecules would occur in between the peptides. The helix would induce a local disordering on the acyl chains, together with bilayer deformation, to better match with the hydrophobic portion of the peptides. Once the bilayer was deformed, with an energetic penalty (Lundbaek *et al.*, 2003), other helices would also be better accommodated nearby, justifying the formation of peptide-enriched patches. Patches with an increased local peptide concentration would, in turn, favor the occurrence of dimers.

These properties of a representative membrane-embedded segment of the AChR, obtained from different fluorescence methodologies, may bear relevance to the organization of the γ-subunit α-helical bundle motif and the AChR membrane-spanning region at large. The tendency of the hydrophobic γM4 peptide to maximize peptide-peptide interactions in the presence but not in the absence of chol may be related to the ability of this sterol to stabilize the α-helix content of the native AChR (Fong and McNamee, 1987; Butler and McNamee, 1993) and to the inability of reconstituted AChR to respond to agonist stimulation with a cation flux in the absence of chol (Rankin *et al.*, 1997).

12.7. PROTEIN/PEPTIDE-LIPID SELECTIVITY: COMPOSITION AND SIZE OF THE ANNULAR REGION

Peptides and proteins interacting with two-component (or multi-component) bilayers are frequently reported to exhibit lipid selectivity, *i.e.*, are preferentially surrounded by one lipid component relative to the other (Dumas *et al.*, 1997; Lehtonen and Kinnunen, 1997; Fahsel *et al.*, 2002). The traditional technique used to address this question has been ESR spectroscopy (*e.g.*, Marsh and Horváth, 1998). However, due to its sensitivity to probe concentration, FRET offers a large potential in this field, and both qualitative (Wang *et al.*, 1988) and quantitative though approximate models (Antollini *et al.*, 1996; Bonini *et al.*, 2002; see Fernandes *et al.* (2004) and Loura *et al.* (2001a) for critical discussions) have been published. In this section, we describe a fluorescence study of lipid selectivity concerning a transmembrane protein for which a new FRET methodology was specifically derived (Fernandes *et al.*, 2004).

As described in the previous section, M13 major coat protein has a single hydrophobic transmembrane segment. Headgroup phospholipid selectivity ESR studies had already been performed with aggregated forms of the protein (Peelen *et al.*, 1992; Wolfs *et al.*, 1989, Datema *et al.*, 1987), pointing to a moderate preference for anionic lipids PA, phosphatiylserine (PS) and PG over zwitterionic lipids PC and PE. This effect most probably results from electrostatic interaction of anionic head groups with the highly basic C-terminal domain of the protein, which contains 4 Lys residues. In the study described below, head group selectivity was studied by FRET from a covalently-bonded fluorophore in the protein (essentially monomeric) to different labeled phospholipids. In addition, selectivity for hydrophobically matching phospholipids relative to non matching counterparts was also investigated.

The FRET model assumes two populations of energy transfer acceptors, one located in a single annular shell around the protein and the other outside the shell. The donor fluorescence decay curve has FRET contributions from both populations:

$$i_{DA}(t) = i_D(t) \cdot \rho_{annular}(t) \cdot \left[\rho_{random}(t)\right]^2 \tag{32}$$

Here i_D and i_{DA} are the donor fluorescence decay in the absence and presence of acceptors respectively, and $\rho_{annular}$ and ρ_{random} are the RET contributions arising from energy transfer to annular labeled lipids and to randomly distributed labeled lipids outside the annular shell respectively.

The acceptors in the annular shell (in our study, (7-nitro-2-1,3-benzoxadiazol-4-yl)amino (NBD)-labeled phospholipids) are located at a constant distance (d) to the fluorophore (in our study, 7-diethylamino-3((4'iodoacetyl)amino)phenyl-4-methyl-coumarin (DCIA), linked at the 36th residue), which lies at the centre of the transmembrane domain (Figure 12.16), and therefore we can assume that the energy transfer to each of these acceptors is described by the rate constant

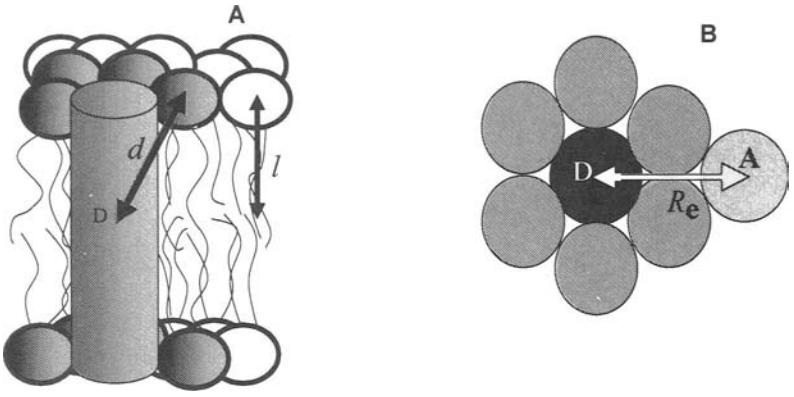

Figure 12.16. Molecular model for the FRET analysis ((A) side view; (B) top view). Protein-lipid organization presents a hexagonal geometry. Donor fluorophore from the mutant protein is located in the center of the bilayer, whereas the acceptors are distributed in the bilayer surface. Two different environments are available for the labeled lipids (acceptors), the annular shell surrounding the protein and the bulk lipid. Energy transfer to acceptors in direct contact with the protein has a rate coefficient dependent on the distance between donor and annular acceptor (Eq. 33). Energy transfer toward acceptors in the bulk lipid is given by Eq. (36) (see text for details). Reprinted with permission from Fernandes *et al.* (2004). Copyright 2004 Biophysical Society.

$$k_J = \frac{1}{\tau_D}\left(\frac{R_0}{d}\right)^6 \tag{33}$$

where τ_D is the donor lifetime (in the absence of acceptor). From spectral data, R_0 = 39.3 Å was measured for this pair. The NBD fluorophores are assumed to be located in the bilayer surface (Chattopadhyay and London, 1987; see also Fernandes *et al.* (2004) for details).

Considering a hexagonal type geometry for the protein-lipid arrangement (Figure 12.16 B), each protein will be surrounded by 12 annular lipids. In bilayers composed by both labeled and unlabeled phospholipids, these 12 sites will be available for both of them. The probability (μ) of one of these sites being occupied by labeled phospholipid is given by

$$\mu = K_S \frac{n_A}{n_A + n_{Lipid}} \tag{34}$$

Here, n_A is the concentration of labeled lipid, and n_{lipid} is the concentration of unlabeled lipid. K_S is the relative association constant, which reports the relative affinity of the labeled and unlabeled phospholipid. Using a binomial distribution, the probability of each occupation number (0-12 sites occupied simultaneously by labeled lipid), and finally the FRET contribution arising from energy transfer to annular lipids is computed,

$$\rho_{annular}(t) = \sum_{n=0}^{n=12} e^{-nk_f \cdot t} \cdot \binom{12}{n} \cdot \mu^n \cdot (1-\mu)^{12-n} \tag{35}$$

The FRET contribution from energy transfer to acceptors randomly distributed outside the annular region in a different plane to that of the donors is given by Davenport *et al.* (1985).

$$\rho_{trans}(t) = \exp\left\{ -2n_2\pi \cdot l^2 \cdot \int_0^{l/\sqrt{l^2+R_e}} \left[1 - \exp(-t\, b^3\, \alpha^6)\right] \alpha^{-3}\, d\alpha \right\} \tag{36}$$

where $b=(R_0/l)^2\tau_D^{-1/3}$, n_2 is the acceptor density in each leaflet, l is the distance between the plane of the donors and the planes of acceptors, and R_e is the distance between the protein axis and the second lipid bilayer (exclusion distance for bulk-located acceptors). For the purpose of this work, n_2 must be corrected for the presence of labeled lipid molecules in the annular region, which therefore are not part of the randomly distributed acceptors pool. After $i_{DA}(t)$ is calculated in Eq. (32), the theoretical energy transfer efficiency E is readily calculated by numerical integration (Eq. 29).

In one experiment, M13 major coat protein selectivity for the acceptor (1,2-dioleoyl-*sn*-glycero-3-phosphoethanolamine derivatized with NBD at the head group) was measured in bilayers of either DOPC, DEuPC or DMoPC. In a second set of measurements, several probes were used as acceptors, all studies being made in DOPC vesicles. The probes used as acceptors were phospholipids of identical acyl chains (18:1 and 12:0) and different head groups (PC, PE, PS, PG, and PA) classes, derivatized with NBD at the 12:0 chain. The complete set of experiments is described in Table 12.6.

Experimental results of FRET efficiency as a function of acceptor concentration are shown (together with the best model fits) in Figures 12.17 and 12.18, and Table 12.6 summarizes the recovered K_S values. Regarding the hydrophobic matching study, the lower value recovered in DOPC relative to those in DMoPC and DEuPC bilayers confirms the larger protein selectivity towards the hydrophobic matching unlabeled phospholipid (DOPC). On the other hand, the varying acceptor head group study, a larger selectivity for the anionic labeled phospholipids (especially the 18:1-(12:0-NBD)-PA and 18:1-(12:0-NBD)-PS probes) is inferred. The latter results confirm those of Peelen *et al.* (1992), obtained using ESR and aggregated protein, and in fact the relative association constants ratios (K_S(PX)/K_S(PC)) obtained in the two works are almost identical.

One important difference between the ESR and FRET techniques is that the latter is not restricted to the lipids adjacent to a given protein molecule. Not only labeled lipids in the first shell of lipids will be potential acceptors to a donor-labeled integral protein, but also the acceptors in the other lipid shells surrounding the protein will contribute to the final result. For that reason, this study also seems to confirm the hypothesis of perturbation (in terms of lipid distribution) induced by the protein to largely limit itself to an annular shell of lipids in direct contact with the protein, in the case of the M13 major coat protein (possibly related to the fact that it has a sole transmembrane segment). Moreover, as commented above, our recovered K_S/K_S(PC) agree with those obtained from ESR measurements, which assume a single layer of annular lipid.

Table 12.6. Relative association constants of labeled phospholipids towards M13 major coat protein.

Labeled phospholipid	Bilayer composition	K_S	$K_S/K_S(PC)^a$
((18:1)2-PE-NBD)	DOPC (18:1)2PC	1.4	—
((18:1)2-PE-NBD)	DEuPC (22:1)2PC	2.1	—
((18:1)2-PE-NBD)	DMoPC (14:1)2PC	2.9	—
(18:1-(12:0-NBD)-PE)	DOPC	2.0	1.0
(18:1-(12:0-NBD)-PC)	DOPC	2.0	1.0
(18:1-(12:0-NBD)-PG)	DOPC	2.3	1.1
(18:1-(12:0-NBD)-PS)	DOPC	2.7	1.3
(18:1-(12:0-NBD)-PA)	DOPC	3.0	1.5

[a] K_S (PC) is the relative association constant of (18:1-(12:0-NBD)-PC).
Reprinted with permission from Fernandes *et al.* (2004). Copyright 2004 Biophysical Society.

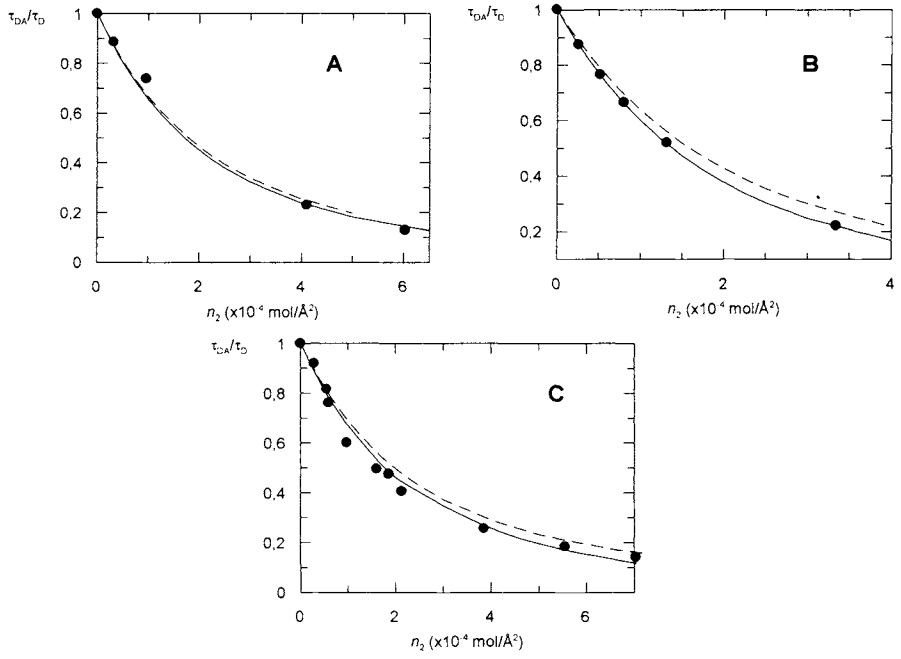

Figure 12.17. Donor (DCIA-labeled protein) fluorescence quenching by FRET acceptor ($(18:1)_2$-PE-NBD) in pure PC bilayers with different hydrophobic thicknesses. (•) - Experimental FRET efficiencies. (—) - Theoretical simulations obtained from the annular model for protein-lipid interaction using the fitted K_S. (---) - Simulations for random distribution of acceptors (K_S = 1.0) - A – Labeled protein incorporated in DOPC (fitted K_S = 1.4); B – Labeled protein incorporated in DMoPC (fitted K_S = 2.9); C – Labeled protein incorporated in DEuPC (fitted K_S = 2.1). Reprinted with permission from Fernandes *et al.* (2004). Copyright 2004 Biophysical Society.

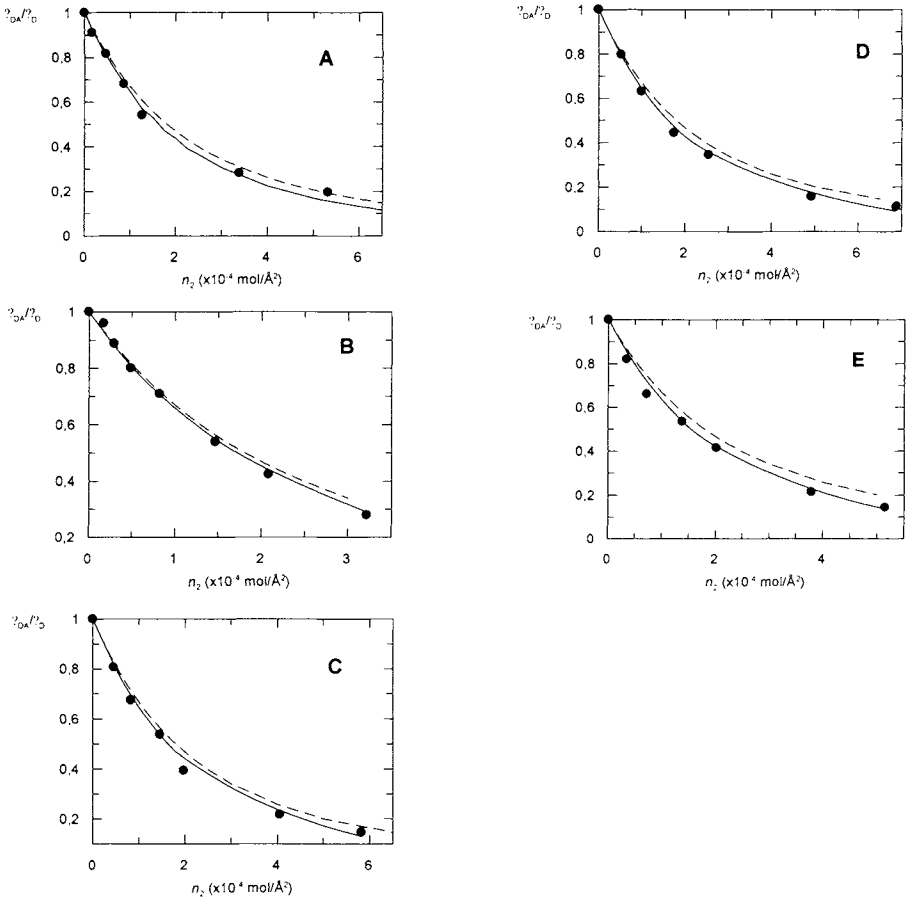

Figure 12.18. Donor (DCIA-labeled protein) fluorescence quenching by energy transfer acceptor (18:1-(12:0-NBD)-PX) (X stands for the different head group structures) in pure bilayers of DOPC. (•) - Experimental energy transfer efficiencies. (—) -Theoretical simulations obtained from the annular model for protein-lipid interaction using the fitted K_S. (---) - Simulations for random distribution of acceptors (K_S = 1.0) - A – PC labeled phospholipid (fitted K_S = 2.0); B - PE labeled phospholipid (fitted K_S = 2.0); C - PG labeled phospholipid (fitted K_S = 2.3); D - PS labeled phospholipid (fitted K_S = 2.7); E - PA labeled phospholipid (fitted K_S = 3.0). Reprinted with permission from Fernandes *et al.* (2004). Copyright 2004 Biophysical Society.

The FRET methodology has three interesting features. Firstly, by choosing donor-acceptors with different Förster radii it is also possible to study mainly the first-shell of lipids or also the outside shells as was the case in the present study. The joint analysis of results coming from these different donor-acceptor pairs could allow for an even more detailed description of the protein-lipid arrangement in more complex systems. In our study, the relatively large R_0 value for the used donor-acceptor pair meant that the experimental quenching curves shown in Figures 12.17 and 12.18 look similar at first sight. It is impressive that the analysis methodology is able to retrieve significant K_S

values nevertheless. Of course, this study could still be improved by the use of a donor-acceptor pair with a smaller R_0 value, closer to the distances under measurement. Second, the more economic character of fluorescence studies, which do not require the same amount of material as ESR, should be stressed. Finally, although this model leads to a somewhat complex decay law, it is actually not necessary to analyze the decay curves with this law to recover the relevant parameters. The theoretical curves are conveniently simulated and integrated in a worksheet in order to calculate the theoretical FRET efficiencies. These can be matched to experimental values by varying the K_S value (the sole unknown parameter). The experimental FRET efficiencies could be obtained from steady-state data. In our case, we obtained them from integration of donor decay curves because these are less prone to artifacts (*e.g.*, light scattering, inner filter effects, measurement of absolute intensities), which in any case, could in principle be corrected for in a steady-state experiment.

12.8. CONCLUDING REMARKS AND ACKNOWLEDGMENTS

In the present review, it was shown how relevant problems in the context of lipid-peptide interaction, such as peptide aggregation, transverse location in the membrane, dynamics, and selectivity for specific lipids can be addressed using fluorescence techniques and methodologies.

Fluorescence spectroscopy is well known in the life sciences due to its intrinsic sensitivity, and this certainly applies to the study of peptides in interaction with membranes, where most of the times minimal amounts of material are available. However, we would like to stress that, in addition to this fact, if topological modeling and state-of-the-art methodologies are used, quantified information regarding both structure and dynamics can be obtained.

Trp and Tyr are present in most membrane-interacting peptide sequences and, in addition, with current technical abilities, alterations on the sequence are trivial and these intrinsic fluorophores can be easily introduced. Although they do have a complex photophysics, such as their fluorescence decay, this can be used to obtain further information on the system. In case that no intrinsic fluorescent residue is present, other residues can be used as quenchers of fluorophores in the membrane, thus providing information on peptide-lipid interaction. A fluorophore group can also be covalently attached to the peptide.

In this moment, in the area of membrane biophysics, the existence of lipid domains, and some related issues such as the role of cholesterol, liquid-ordered phases and the existence of "rafts" are the leading areas of research. Regarding membrane domains, the simpler models are the binary lipid systems. A quantitative global treatment of the peptide photophysics taking into account phase separation is seldom carried out. This would imply, *e.g.*, the determination of the partition coefficient of the peptide between the lipid phases, and the consequences of the presence of the domains, such as different peptide aggregation states. In the present work illustrative cases both in binary and one-phase systems were described in detail.

Finally we acknowledge Fundação para a Ciência e a Tecnologia (Portugal) for financial support, namely projects and R.F.M. de A.'s grant (SFRH/BD/943/2000) under the program POCTI. We also want to thank the other co-authors of our cited work.

12.9. REFERENCES

Abrams, F. S., and London, E., 1992, Calibration of the parallax fluorescence quenching method for the determination of membrane penetration depth: refinement and comparison of quenching by spin-labelled probes, *Biochemistry* **31**:5312.

Almgren, M., 1991, Kinetics of excited state processes in micellar media, in: *Kinetics and Catalysis in Microheterogeneous Systems*. M. Gratzel and K. Kalyanasundaram, eds., Marcell Dekker, New York, pp. 63-113.

Al-Obeidi, F., Castrucci, A. M. L., Hadley, M. E., and Hruby, V. J., 1989, Potent and prolonged acting cyclic lactam analogues of α-melanotropin: design based on molecular dynamics, *J. Med. Chem.* **32**:2555.

Antollini, S. S., Soto, M. A., Bonini de Romanelli, I., Gutierrez-Merino, C., Sotomayor, P., and Barrantes, F. J., 1996, Physical state of bulk and protein-associated lipid in nicotinic acetylcholine receptor-rich membrane studied by laurdan generalized polarization and fluorescence energy transfer, *Biophys. J.* **70**:1275.

Barrantes, F. J., Antollini, S. S., Blanton, M. P., and Prieto, M., 2000, Topography of nicotinic acetylcholine receptor membrane-embedded domains, *J. Biol. Chem.* **275**:37333.

Berberan-Santos, M. N., and Prieto, M. J. E., 1987, Energy transfer in spherical geometry. Application to micelles, *J. Chem. Soc. Faraday Trans. 2* **83**:1391.

Berberan-Santos, M. N., and Valeur, B., 1991, Fluorescence depolarization by electronic energy transfer in donor-acceptor pairs of like and unlike chromophores, *J. Chem. Phys.* **95**:8048.

Best, L., John, E., and Jähnig, F., 1987, Order and fluidity of lipid membranes as determined by fluorescence anisotropy decays, *Eur. Biophys. J.* **15**:87.

Biaggi, M. H, Riske, K. A., and Lamy-Freund, M. T., 1997, Melanotropic peptides-lipid bilayer interaction. Comparison of the hormone α-MSH to a biologically more potent analog, *Biophys. Chem.* **67**:139.

Blatt, E., Chatelier, R. C., and Sawyer, W. H., 1984, The transverse location of fluorophores in lipid bilayers and micelles as determined by fluorescence techniques. *Photochem. Photobiol.* **39**:477.

Bloom, M., and Mouritsen, O. G., 1995, The evolution of membranes, in: *Handbook of Biological Physics, vol. 1A: Structure and Dynamics of Membranes - from Cells to Vesicles*. R. Lipowsky, E. Sackmann, eds., Elsevier Science B.V., Amsterdam, pp. 65-95.

Bonini, I. C., Antollini, S. S., Gutierrez-Merino, C., and Barrantes, F. J., 2002, Sphingomyelin composition and physical asymmetries in native acetylcholine receptor-rich membranes, *Eur. Biophys. J.* **31**:417.

Bowie, J. U., 1997, Helix packing in membrane proteins, *J. Mol. Biol.* **272**:780.

Brown, D. A., and London, E., 2000, Structure and function of sphingolipid- and cholesterol-rich membrane rafts, *J. Biol. Chem.* **275**:17221.

Butler, D. H., and McNamee, M. G., 1993, FTIR analysis of nicotinic acetylcholine receptor secondary structure in reconstituted membranes, *Biochim. Biophys. Acta* **1150**:17.

Castanho, M. A. R. B., and Prieto, 1992, Fluorescence study of the macrolide pentaene antibiotic filipin in aqueous solution and in a model system of membranes, *Eur. J. Biochem.* **207**:125.

Castanho, M. A. R. B., Prieto, M., and Acuña, A. U., 1996, The tranverse location of the fluorescent probe *t*-parinaric acid in lipid bilayers, *Biochim. Biophys. Acta* **1279**:164.

Chattopadhyay, A., 2003, Exploring membrane organization and dynamics by the wavelength-selective fluorescemce approach, *Chem. Phys. Lipids* **122**:3.

Chattopadhyay, A., and London, E., 1987, Parallax method for direct measurement of membrane penetration depth utilizing fluorescence quenching by spin-labelled phospholipids, *Biochemistry* **26**:1987,39.

Chen, R., and Bowman, R. L., 1965, Fluorescence polarization: measurement with ultraviolet-polarizing filters in a spectrophotofluorometer, *Science* **147**:729.

Chen, Y., and Barkley, M. D., 1998, Toward understanding tryptophan fluorescence in proteins, *Biochemistry* **37**:9976.

Chiu, S.-W., Jakobson, E., Subramaniam, S., and Scott, H. L., 1999, Combined Monte Carlo and molecular dynamics simulation of fully hydrated dioleoyl and palmitoyl-oleyl phosphatidylcholine lipid bilayers, *Biophys. J.* **77**:2462.

Contreras, L. M., de Almeida, R. F. M., Villalaín, J., Fedorov, A., and Prieto, M., 2001, Interaction of α-melanocyte stimulating hormone with binary phospholipids membranes: structural changes and relevance of phase behaviour, *Biophys. J.* **80**:2273.

Dahms, T. E. S., and Szabo, A. G., 1995, Probing local secondary structure by fluorescence: time-resolved and circular dichroism studies of highly purified neurotoxins, *Biophys. J.* **69**:569.

Datema, K. P., Wolfs, C. J. A. M., Marsh, D., Watts, A., and Hemminga, M. A., 1987, Spin label electron spin resonance study of bacteriophage M13 coat protein incorporation into mixed lipid bilayers, *Biochemistry* **26**:7571.

Davenport, L., Dale, R. E., Bisby, R. H., and Cundall., R. B., 1985, Transverse location of the fluorescent probe 1,6-diphenyl-1,3,5-hexatriene in model lipid bilayer membrane systems by resonance energy transfer, *Biochemistry* **24**:4097.

de Almeida, R. F. M., Loura, L. M. S., Fedorov, A., and Prieto, M., 2002, Non-equilibrium phenomena in the phase separation of a two-component lipid bilayer, *Biophys. J.* **82**:823.

de Almeida, R. F. M., Fedorov, A., and Prieto, M., 2003, Sphingomyelin / phosphatidylcholine / cholesterol phase diagram: boundaries and composition of lipid rafts, *Biophys. J.* **85**:2406.

de Almeida, R. F. M., Loura, L. M. S., Prieto, M., Watts, A., Fedorov, A., and Barrantes, F. J., 2004, Cholesterol modulates the organization of the γM4 transmembrane domain of the muscle nicotinic acetylcholine receptor, *Biophys. J.* **86**:2261.

de Planque, M. R. R., Kruijtzer, J. A. W., Liskamp, R. M. J., Marsh, D., Greathouse, D. V., Koeppe II, R. E., de Kruijff, B., and Killian, J. A., 1999, Different membrane anchoring positions of tryptophan and lysine in synthetic transmembrane alpha-helical peptides, *J. Biol. Chem.* **274**:20839.

Dietrich, C., Bagatolli, L. A., Volovyk, Z. N., Thompson, N. L., Levi, M., Jacobson, K., and Gratton, E., 2001, Lipid rafts reconstituted in model membranes, *Biophys. J.* **80**:1417.

Dumas, F., Sperotto, M. M., Lebrun, M.-C., Tocanne, J.-F., and Mouritsen, O. G., 1997, Molecular sorting of lipids by bacteriorhodopsin in dilauroylphosphatidylcholine /distearoylphosphatidylcholine lipid bilayers, *Biophys. J.* **73**:1940.

Eberle, A. N., 1988, *The Melanotropins. Chemistry, Physiology and Mechanism of Action*, Karger Publishers, Basel.

Edidin, M., 1998, Defining and imaging membrane domains. *Biol. Skr. Dan. Vid. Selsk.* **49**:19.

Edidin, M., 2003, Lipids on the frontier: a century of cell-membrane bilayers, *Nat. Rev. Mol. Cell Biol.* **4**:414.

Eisinger, J., Blumberg, W. E., and Dale, R. E., 1981, Orientational effect in intra- and intermolecular long range excitation energy transfer, *Ann. N. Y. Acad. Sci.* **366**:155.

Engelborghs, Y., 2001, The analysis of time resolved protein fluorescence in multi-tryptophan proteins, *Spectrochim. Acta A Mol. Biomol. Spectrosc.* **57**:2255.

Fahsel, S., Pospiech, E. M., Zein, M., Hazlet, T. L., Gratton, E., and Winter, R., 2002, Modulation of concentration fluctuations in phase separated lipid membranes by polypeptide insertion, *Biophys. J.* **83**:334.

Fernandes, F., Loura, L. M. S., Prieto, M., Koehorst, R., Spruijt, R. B., and Hemminga, M. A., 2003, Dependence of M13 major coat protein oligomerization and lateral segregation on bilayer composition, *Biophys. J.* **85**:2430.

Fernandes, F., Loura, L. M. S., Koehorst, R., Spruijt, R. B., Hemminga, M. A., Fedorov, A., and Prieto, M., 2004, Quantification of protein-lipid selectivity using FRET: application to the M13 major coat protein, *Biophys. J.* **87**:344.

Fernandes, M. X., García de la Torre, J., and Castanho, M. A. R. B., 2002, Joint determination by Brownian dynamics and fluorescente quanching of the in-depth location profila of biomolecules in membranes, *Anal. Biochem.* **307**:1.

Ferreira, S. T., Stella, L., and Gratton, E., 1994, Conformational dynamics of bovine Cu, Zn superoxide dismutase revealed by time-resolved fluorescence spectroscopy of the single tyrosine residue, *Biophys. J.* 7:1185.

Fong, T. M., and McNamee, M. G., 1987, Stabilization of acetylcholine receptor secondary structure by cholesterol and negatively charged phospholipids in membranes, *Biochemistry* **26**:3871.

Graham, I. G., Gagné, J., and Silvius, J. R., 1985, Kinetics and thermodynamics of calcium induced lateral phase separations in phosphatidic acid containing bilayers, *Biochemistry* **24**:7123.

Gryczynski, I., Steiner, R. F., and Lakowicz, J. R., 1991, Intensity and anisotropy decays of the tyrosine calmodulin proteolytic fragments, as studied by GHz frequency-domain fluorescence, *Biophys. Chem.* **39**:69.

Hemminga, M. A., Sanders, J. C., Wolfs, C. J. A. M., and Spruijt, R. B., 1993, Lipid-protein interactions involved in bacteriophage M13 infection, *Protein-Lipid Inter. New Compr. Biochem.* **25**:191.

Hoshi, T., Zagotta, W. N., and Aldrich, R. W., 1990, Biophysical and molecular mechanisms of Shaker potassium channel inactivation, *Science* **250**:533.

Hruby, V. J., Wilkes, B. C., Hadley, M. E., Al-Obeidi, F., Sawyer, T. K., Staples, D. G., deVaux, A. E., Dym, O., Castrucci, A. M. de L., Hintz, M. F., Riehm, J. P., and Rao, R., 1987, α-Melanotropin: the minimal active sequence in the frog skin bioassay, *J. Med. Chem.* **30**:2126-2130.

Hurley, J. H., and Meyer, T., 2001, Subcellular targeting by membrane lipids, *Curr. Opin. Cell. Biol.* **13**:146-152.

Ipsen, J. H., Karlström, G., Mouritsen, O. G., Wennerström, H., and Zuckermann, M. J., 1987, Phase equilibria in the phosphatidylcholine-cholesterol system, *Biochim. Biophys. Acta* **905**:162-172.

Ito, A. S., Castrucci, A. M. de L., Hruby, V. J., Hadley, M. E., Krajcarski, D. T., and Szabo, A. G., 1993, Structure-activity correlations of melanotropin peptides in model lipids by tryptophan fluorescence studies, *Biochemistry* **32**:12264.

Jabłoński, A., 1960, On the notion of emission anisotropy, *Bull. Acad. Pol. Sci.* **8**:259.

Johnson, J. E., and Cornell, R. B., 1999, Amphitropic proteins: regulation by reversible membrane interactions, *Mol. Membr. Biol.* **16**:217.

Killian, J. A., 1998, Hydrophobic mismatch between proteins and lipids in membranes, *Biochim. Biophys. Acta* **1376**:401.

Kinosita, K., Jr., Ikegami, A., and Kawato, S., 1982, On the wobbling-in-cone analysis of fluorescence anisotropy decay, *Biophys. J.* **37**:461.

Korlach, J., Schwille, P., Webb, W. W., and Feigenson, G. W., 1999, Characterization of lipid bilayer phases by confocal microscopy and fluorescence correlation spectroscopy, *Proc. Natl. Acad. Sci. USA* **96**:8461.

Ladokhin, A. S., 1997, Distribution analysis of depth-dependent fluorescence quenching in membranes. *Meth. Enzymol.* **278**:462.

Ladokhin, A. S., 2001, On the interpretation of decay-associated fluorescence spectra in proteins, *Biopolymers Cell* **17**:221.

Lafleur, M., Faucon, J. F., Dufourcq, J., and Pezolet, M., 1989, Perturbation of binary phospholipid mixtures by melittin: a fluorescence and Raman spectroscopy study, *Biochim. Biophys. Acta* **980**:85.

Lakowicz, J. R., 1999, *Principles of Fluorescence Spectroscopy*, 2nd Ed., Kluwer Academic/Plenum Press, New York.

Lakowicz, J.R., 2000, On spectral relaxation in proteins, *Photochem. Photobiol.* **72**:421.

Laws, W. R., Ross, J. B. A., Wyssbrod, H. R., Beechem, J. M., Brand, L., Sutherland, J. C., 1986, Time-resolved fluorescence and ^{1}H-NMR studies of tyrosine and tyrosine analogues: correlation of NMR-determined rotamer populations and fluorescence kinetics, *Biochemistry* **25**:599.

Lehrer, S. S., 1971, Solute perturbation of protein fluorescence. The quenching of the tryptophanyl fluorescence of model compounds and of lysozime by iodide ion. *Biochemistry* **10**:3254.

Lehtonen, J. Y. A., and Kinnunen, P. K. J., 1997, Evidence for phospholipids microdomain formation in liquid crystalline liposomes reconstituted with *Escherichia coli* lactose permease, *Biophys. J.* **72**:1247.

Lehtonen, J. Y. A., Holopainen, J. M., and Kinnunen, P. K. J., 1996, Evidence for the formation of microdomains in liquid crystalline large unilamellar vesicles caused by hydrophobic mismatch of the constituent phospholipids, *Biophys. J.* **70**:1753.

Lentz, B. R., Barrow, D. A., and Hoechli, M., 1980, Cholesterol-phosphatidylcholine interactions in multilamellar vesicles, *Biochemistry* **19**:1943.

Lewis, B. A., and Engelman, D. M., 1983, Bacteriorhodopsin remains dispersed in fluid phospholipid bilayers over a wide range of bilayer thickness, *J. Mol. Biol.* **166**:203.

Lipari, G., and Szabo, A., 1980, Effect of vibrational motion on fluorescence depolarization and nuclear magnetic resonance relaxation in macromolecules and membranes, *Biophys. J.* **30**:489.

London, E., and Brown, D. A., 2000, Insolubility of lipids in triton X-100: physical origin and relationship to sphingolipid/cholesterol membrane domains (rafts), *Biochim. Biophys. Acta* **1508**:182.

Loura, L. M. S., and Prieto, M., 1997, Dehydroergosterol structural organization in aqueous medium and in a model system of membranes, *Biophys. J.* **72**:2226.

Loura, L. M. S., Fedorov, A., and Prieto, M., 1996, Resonance energy transfer in a model system of membranes: application to gel and liquid crystalline phases, *Biophys. J.* **71**:1823.

Loura, L. M. S., Fedorov, A., and Prieto, M., 2000, Membrane probe distribution heterogeneity: a resonance energy transfer study, *J. Phys. Chem. B.* **104**:6920.

Loura, L. M. S., de Almeida, R. F. M., and Prieto, M., 2001a, Detection and characterization of membrane microheterogeneity by resonance energy transfer, *J. Fluoresc.* **11**:197.

Loura, L. M. S., Fedorov, A., and Prieto, M., 2001b, Exclusion of a cholesterol analog from the cholesterol-rich phase in model membranes, *Biochim. Biophys. Acta* **1511**:236.

Loura, L. M. S., de Almeida, R. F. M., Coutinho, A., and Prieto, M., 2003, Interaction of peptides with binary phospholipid membranes: application of fluorescence methodologies, *Chem. Phys. Lipids* **122**:77.

Lundbaek, J. A., Anderson, O. S., Werge, T., and Nielsen, C., 2003, Cholesterol-induced protein sorting: an analysis of energetic feasibility, *Biophys. J.* **84**:2080.

Mabrey, S., and Sturtevant, J. M., 1976, Investigation of phase transitions of lipids and lipid mixtures by high-sensitivity differential scanning calorimetry, *Proc. Natl. Acad. Sci. USA*. 73:3862.

Mall, S., Broadbridge, R., Sharma, R. P., East, J. M., and Lee, A. G., 2001, Self-association of model transmembrane helix is modulated by lipid structure, *Biochemistry* **40**:12379.

Marsh, D., 1990, *Handbook of Lipid Bilayers*, CRC Press, Boca Raton.

Marsh, D., and Horváth, L. I., 1998, Structure, dynamics and composition of the lipid-protein interface. Perspectives from spin-labelling, *Biochim. Biophys. Acta* **1376**: 267.

Mateo, C. R., Acuña, A. U., and Brochon, J.-C., 1995, Liquid-crystalline phases of cholesterol/lipid bilayers as revealed by the fluorescence of *trans*-parinaric acid, *Biophys. J.* **68**:978.

Mateo, C. R., Souto, A. A., Amat-Guerri, F., and Acuña, U., 1996, New fluorescent octadecapentaenoic acids as probes of lipid membranes and protein-lipid interactions *Biophys. J.* **71**:2177.

McMullen, T. P. W., and McElhaney, R. N., 1995, New aspects of the interaction of cholesterol with dipalmitoylphosphatidylcholine bilayers as revealed by high-sensitivity differential scanning calorimetry, *Biochim. Biophys. Acta* **1234**:90.

Meijer, A. B., Spruijt, R. B., Wolfs, C. J. A. M., and Hemminga, M. A. 2001, Membrane-anchoring interactions of M13 major coat protein, *Biochemistry* **40**:8815.

Milhiet, P. E., Domec, C., Giocondi, M.-C., Van Mau, N., Heitz, F., and Le Grimellec, C., 2001, Domain formation in models of the renal brush border membrane outer leaflet, *Biophys. J.* **81**:547.

Mobashery, N., Nielsen, C., and Andersen, O. S., 1997, The conformational preference of gramicidin channels is a function of lipid bilayer thickness, *FEBS Lett.* **412**:15.

Moreno, M. J., and Prieto, M., 1993, Interaction of the peptide hormone adrenocorticotropin, ACTH (1-24), with a membrane model system: a fluorescence study, *Photochem. Photobiol.* **57**:431.

Mouritsen, O. G., and Bloom, M., 1984, Mattress model of lipid-protein interactions in membranes, *Biophys. J.* **46**:141.

Mouritsen, O. G., and Jørgensen, K. 1994, Dynamical order and disorder in lipid bilayers, *Chem. Phys. Lipids* **73**:3.

Mouritsen, O. G., and Jørgensen, K., 1997, Small-scale lipid-membrane structure: simulation vs. experiment, *Curr. Opin. Struct. Biol.* 7:518.

Needham, D., and Nunn, R. S., 1990, Cohesive properties (elastic deformation and failure) of lipid bilayer membranes containing cholesterol, *Biophys. J.* **58**, 997.

Nezil, F. A., and Bloom, M., 1992, Combined influence of cholesterol and synthetic amphiphilic peptides upon bilayer thickness in model membranes, *Biophys. J.* **61**:1176.

Owen, C. S., 1975, Two dimensional diffusion theory: cylindrical diffusion model applied to fluorescence quenching, *J. Chem. Phys.* **62**:3204.

Pascutti, P. G., El-Jaik, L. J., Bisch, P. M., Mundim, K. C., and Ito, A. S., 1999, Molecular dynamics simulation of α-melanocyte stimulating hormone in a water-membrane model interface, *Eur. Biophys. J.* **28**:499.

Peelen, S. J. C. J., Sanders, J. C., Hemminga, M. A., and Marsh, D., 1992, Stoichiometry, selectivity and exchange dynamics of lipid-protein interaction with bacteriophage M13 coat protein studied by spin label electron spin resonance. Effects of protein secondary structure, *Biochemistry* **31**:2670.

Perrin, F., 1926, Polarization de la lumière de fluorescence. Vie moyenne des molécules dans l'état excité, *J. Phys. Radium* 7:390.

Perrin, F., 1929, La fluorescence des solutions: induction moléculaire, polarization et durée d'émission, *Ann. Phys. (Paris)* **12**:169.

Poveda, J. A., Prieto, M., Encinar, J. A., González-Ros, J. M., and Mateo, C. R., 2003, Intrinsic tyrosine fluorescence as a tool to study the interaction of the Shaker B "ball" peptide with anionic membranes, *Biochemistry* **42**:7124.

Rankin, S. E., Addona, G. H., Kloczewiak, M. A. Bugge, B., and Miller, K. W., 1997, The cholesterol dependence of activation and fast desensitization of the nicotinic acetylcholine receptor, *Biophys. J.* **73**:2446.

Razi-Naqvi, K., 1974, Diffusion-controlled reactions in two dimensional fluids: discussion of measurements of lateral diffusion of lipids in biological membranes, *Chem. Phys. Lett.* **28**:2303.

Ren, J., Lew, S., Wang, J., and London, E. 1999, Control of the transmembrane orientation and interhelical interactions within membranes by hydrophobic helix length, *Biochemistry* **38**:5905.

Runnels, L. W., and Scarlata, S. F., 1995, Theory and application of fluorescence homotransfer to melittin oligomerization, *Biophys. J.* **69**:1569.

Russel, M., 1991, Filamentous phage assembly, *Mol. Microbiol.* **5**:1607.

Sanders, J. C., van Nuland, N. A. J., Edholm, O., and Hemminga, M., 1991, Conformational and aggregation of M13 coat protein studied by molecular dynamics, *Biophys. Chem.* **41**:193-202.

Santos, N. C., Prieto, M., and Castanho, M. A. R. B., 1998, Interaction of the major epitope region of HIV protein gp41 with membrane model systems. A fluorescence spectroscopy study, *Biochemistry* **37**:8674.

Santos, N. C., Prieto, M., and Castanho, M. A. R. B., 2003, Quantifying molecular partition into model systems of biomembranes: an emphasis on optical spectroscopic methods, *Biochim. Biophys. Acta* **1612**:123.

Sawyer, T. K., Sanfilippo, P. J., Hruby, V. J., Engel, M. H., Heward, C. B., Burnett, K. B., and Hadley, M. E., 1980, 4-Norleucine, 7-D-phenylalanine-α-melanocyte-stimulating hormone: a highly potent α-melanotropin with ultralong biological activity, *Proc. Natl. Acad. Sci. USA* 77:5754.

Sawyer, T. K., Hruby, V. J., Darman, P. S., and Hadley, M. E., 1982, [half-Cys^4,half-Cys^{20}]-α-melanocyte-stimulating hormone: a cyclic α-melanotropin exhibiting superagonist biological activity, *Proc. Natl. Acad. Sci. USA* **79**:1751.

Sillen, A., and Engelborghs, Y., 1998, The correct use of "average" fluorescence parameters, *Photochem. Photobiol.* **67**:475.

Silvius, J. R., 1992, Cholesterol modulation of lipid intermixing in phospholipid and glycosphingolipid mixtures. Evaluation using fluorescent lipid probes and brominated lipid quenchers, *Biochemistry* **31**:3398.

Simon, J. A., Williamson, I. M., East, J. M., and Lee, A. G., 2003, Interactions of anionic phospholipids and phosphatidylethanolamine with the potassium channel KcsA. *Biophys. J.* **85**:3828.

Simons, K., and Ikonen, E., 1997, Functional rafts in cell membranes, *Nature* **387**:569.

Singer, S. J., and Nicolson, G. L., 1972, The fluid mosaic model of the structure of cell membranes, *Science* 175:720.

Smaby, J. M., Momsen, M. M., Brockman, H. L., and Brown, R. E., 1997, Phosphatidylcholine acyl unsaturation modulates the decrease in interfacial elasticity induced by cholesterol, *Biophys. J.* **73**:1492.

Small, D. M., 1986, *The Physical Chemistry of Lipids: from Alkanes to Phospholipids (Handbook of Lipid Research, Vol. 4)*. Plenum Press, New York.

Smith, L. M., Smith, B. A., and McConnell, H. M., 1979, Lateral diffusion of M-13 coat protein in model membranes, *Biochemistry* **18**:2256.

Smith, L. M., Rubenstein, J. L. R., Parce, J. W., and McConnell, H. M., 1980, Lateral diffusion of M-13 coat protein in mixtures of phosphatidylcholine and cholesterol, *Biochemistry* **19**:5907.

Snyder, B., and Freire, E., 1982, Fluorescence energy transfer in two dimensions. A numeric solution for random and non-random distributions, *Biophys. J.* **40**:137.

Spruijt, R. B., Wolfs, C. J. A. M., and Hemminga, M. A., 1989, Aggregation related conformational change of the membrane-associated coat protein of bacteriophage M13, *Biochemistry* **28**:9158.

Stopar, D., Spruijt, R. B., Wolfs, C. J. A. M., and Hemminga, M. A., 1997, In situ aggregational state of M13 bacteriophage major coat protein in sodium cholate and lipid bilayers, *Biochemistry* **36**:12268.

Stopar, D., Spruijt, R. B., Wolfs, C. J. A. M., and Hemminga, M. A., 2003, Protein-lipid interactions of bacteriophage M13 major coat protein, *Biochim. Biophys. Acta* **1611**:5.

Szabo, A. G. and Rayner, D. M., 1980, The time resolved emission spectra of peptide conformers measured by pulsed laser excitation, *Biochem. Biophys. Res. Commun.* **94**:909.

Tanaka, F., Tamai, N., Mataga, N., Tonomura, B., and Hiromi, K., 1994, Analysis of internal motion of single tryptophan in *Streptomyces* subtilisin inhibitor from its picosecond time-resolved fluorescence, *Biophys. J.* **67**: 874.

Thewalt, J. L., and Bloom, M., 1992, Phosphatidylcholine: cholesterol phase diagrams. *Biophys. J.* **63**:1176.

Toptygin, D., Savtchenko, R. S., Meadow, N. D., and Brand, L., 2001, Homogeneous spectrally- and time-resolved fluorescence emission from single-tryptophan mutants of IIA^{Glc} Protein. *J. Phys. Chem. B* **105**:2043.

Tristam-Nagle, S., Petrache, H. I., and Nagle, J. F., 1998, Structure and interactions of fully hydrated dioleoylphosphatidylcholine bilayers, *Biophys. J.* **75**:917.

Umberger, J. Q., and Lamer, V. K., 1945, The kinetics of diffusion controlled molecular and ionic reactions in solution as determined by measurements of the quenching of fluorescence, *J. Am. Chem. Soc.* **67**:1099.

Valeur, B., 2001, *Molecular Fluorescence. Principles and Applications*, Wiley-VCH, New York.

Valeur, B., and Weber, G., 1977, Anisotropic rotations in 1-naphthylamine, existence of a red-edge transition moment normal to the ring plane, *Chem. Phys. Lett.* **45**:140.

Valeur, B., and Weber, G., 1977, Resolution of the fluorescence excitation spectrum of indole into the ^1L_a and ^1L_b excitation bands, *Photochem. Photobiol.* **25**:441.

Vaz, W. L. C., Criado, M., Madeira, V. M. C., Schoellmann, G., and Amd Jovin, T. M., 1982, Size dependence of the translational diffusion of large integral membrane proteins in liquid-crystalline phase lipid bilayers. A study using fluorescence recovery after photobleaching, *Biochemistry* **21**:5608.

Villalaín, J. B., and Prieto, M., 1991, Location and interaction of n-(9-anthroyloxy)-stearic acid probes incorporated in phosphatidylcholine vesicles, *Chem. Phys. Lipids* **59**:9.

Vincent, M., Gilles, A.-M., de la Sierra, I. M. L., Briozzo, P., Bârzu, O., Gallay, J., 2000, Nanosecond fluorescence dynamic stokes shift of tryptophan in a protein matrix, *J. Phys. Chem. B* **104**:11286.

Vist, M. R., and Davis, J. H., 1990, Phase equilibria of cholesterol/dipalmitoylphosphatidylcholine mixtures: ^2H nuclear magnetic resonance and differential scanning calorimetry, *Biochemistry* **29**:451.

Vogel, H., Nilsson, L., Rigler, R., Vogues, K.-L., and Jung, G., 1988, Structural fluctuations of a helical polypeptide traversing a lipid bilayer, *Proc. Natl. Acad. Sci. USA* **85**:5067.

Wang, S., Martin, E., Cimino, J., Omann, G., Glaser, M., 1988, Distribution of phospholipids around gramicidin and D-beta-hydroxybutyrate dehydrogenase as measured by resonance energy transfer, *Biochemistry* **27**:2033.

Weber, G., 1960, Fluorescence-polarization spectrum and electronic electronic-energy transfer in tyrosine, tryptophan and related compounds, *Biochem. J.* **75**:335.

Weber, G., and Shinitzky, M., 1970, Failure of energy transfer between identical aromatic molecules on excitation at the long wave edge of the absorption spectrum, *Proc. Natl. Acad. Sci. USA* **65**:823.

Welti, R., and Glaser, M., 1994, Lipid domains in model and biological membranes, *Chem. Phys. Lipids* **73**:121.

Wiener, M. C., and White, S. H., 1992, Structure of a fluid dioleoylphosphatidylcholine bilayer determined by joint refinement of x-ray and neutron diffraction data. III. Complete structure, *Biophys. J.* **61**:437.

Willis, K. J., and Szabo, A. G., 1992, Conformation of parathyroid hormone: time-resolved fluorescence studies, *Biochemistry* **31**:8924.

Wimley, W. C., and White, S. H., 1996, Experimentally determined hydrophobicity scale for proteins at membrane interfaces, *Nat. Struct. Biol.* **3**:842.

Wolber, P. K., and Hudson, B. S., 1979, An analytical solution to the Förster energy transfer problem in two dimensions, *Biophys. J.* **28**:197.

Wolfs, C. L. A. M., Horváth, L. I., Marsh, D., Watts, A., Hemminga, M. A., 1989, Spin label ESR of bacteriophage M13 coat protein in mixed lipid bilayers. Characterization of molecular selectivity of charged phospholipids for the bacteriophage M13 coat protein in lipid bilayers, *Biochemistry* **28**:995.

Wu, S. H., and McConnell, H. M., 1975, Phase separations in phospholipid membranes, *Biochemistry* **14**:847.

Zamyatnin, A. A., 1972, Protein volume in solution, *Prog. Biophys. Mol. Biol.* **24**:107.